1 A Study on the Fully Coupled Atmosphere-Land-Hydrology Process and 2 Streamflow Simulations over the Source Region of the Yellow River

3 Yaling Chen[1], Jun Wen[1], Xianhong Meng[2], Qiang Zhang[1], Xiaoyue Li[1], Ge Zhang[1]

4 [1]Key Laboratory of Plateau Atmosphere and Environment, Sichuan Province, College of Atmospheric Sciences, Chengdu
5 University of Information Technology, Chengdu 610225, China

6 [2]Key Laboratory of Land Surface Process and Climate Change in Cold and Arid Regions, Northwest Institute of Eco-
7 Environment and Resources, Chinese Academy of Sciences, Lanzhou 730000, China

8 *Correspondence to*: Jun Wen (jwen@cuit.edu.cn)

9 **Abstract.** The Source Region of the Yellow River (SRYR) is known as the "Water Tower of the Yellow River", which is the
10 most important water conservation area in the upper reaches of the Yellow River. The streamflow of the SRYR makes an
11 important contribution to the water resources in the Yellow River basin. Based on the Weather Research and Forecasting
12 Model Hydrological modeling system (WRF-Hydro) model, by using meteorological, hydrological observations and
13 reanalysis data, the key variables of the coupled atmosphere-land-hydrological processes over the SRYR during the 2013
14 rainy season (May-August) are analyzed, and the simulation results of the fully coupled WRF-Hydro with those of the
15 standalone WRF are compared, whose aim is to assess the impact of hydrological coupling on the regional atmospheric
16 model settings. The results show that the WRF-Hydro model has ability to depict the characteristics of streamflow over the
17 SRYR with a Nash Efficiency Coefficient (NSE) of 0.44 during the calibration period from June 1st , 2012 to September 30th,
18 2012 and a NSE of 0.61 during the validation period from May 1st, 2013 to August 31st, 2013. Compared with the standalone
19 WRF model, the fully coupled model tends to show better performance with respect to temperature, downward longwave
20 radiation, downward shortwave radiation, latent heat, sensible heat and soil temperature and moisture. Although the wet bias
21 of the coupled simulated precipitation slightly increases (2.51 mm vs. 2.50 mm) due to the consideration of lateral flow of
22 soil water, the simulation results of the land-atmosphere water-heat exchange fluxes and soil heat fluxes are comparably
23 improved. Compared with the observations, the mean Root Mean Square Error (RMSE) of latent and sensible heat is reduced
24 to 32.27 W·m^{-2} and 24.91 W·m^{-2}, and of surface soil temperature and moisture is reduced to 4.22 K and 0.06 m^3/m^3. Besides,
25 the fully coupled model is able to capture the variation characteristics of streamflow with a NSE of 0.33, which indicates that
26 the fully coupled WRF-Hydro model has great potential for characterizing coupled atmosphere-land-hydrological processes
27 and streamflow simulation in the cold climatical and complex topographic regions.

1 Introduction

29 Water, energy and heat flux and the processes among the atmosphere, land surface and hydrology are closely linked through
30 highly complex interactions (Arnault et al., 2016; Fersch et al., 2020). In the water cycle of the whole Earth Climate System,
31 the land surface hydrological processes are the link between atmospheric water (e.g. precipitation, evapotranspiration, water

32 vapor transport), terrestrial surface water (e.g. rivers, lakes, glacial meltwater, snow meltwater, surface runoff, oceans),

33 groundwater (e.g. baseflow, subsurface runoff, soil water), and ecological water (vegetation water), which is able to provide

34 feedback to weather and climate by regulating land-atmosphere energy and water cycle processes (Zheng et al., 2020).

35 Therefore, understanding the hydrological cycle processes between the atmosphere and the land surface in the mesoscale

36 river basins is of great importance for local ecological protection and macro regulation of water resources (Milly et al., 2005).

37 The Source Region of the Yellow River (SRYR) is located in the hinterland of the Tibetan Plateau (TP). It belongs to the

38 continental semi-arid climate zone of the plateau, with complex climatic conditions and the temperature rise rate of

39 0.48 °C/(10a)$^{-1}$ and precipitation increase of 7.6 mm/(10a)$^{-1}$ (Meng et al., 2020). The region is sensitive and fragile to climate

40 change and ecological environment, with a large number of alpine lakes, wetlands, which is the "sensitive area" and "start-up

41 area" for East Asia and even global climate change (Wu et al., 2004). The SRYR is known as "Yellow River Water Tower"

42 and accounts for about 16.2% of the total area of the Yellow River Basin. The streamflow is dominated by precipitation and

43 glacial meltwater and is the main flow-producing area and water conservation area of the middle and upper reaches of the

44 Yellow River (Zheng et al., 2007). Historic records prove that the Yellow River civilization has been able to continue for

45 thousands of years, one of the important reasons is that there is a stable ecological environment and water supply of the

46 SRYR (Zhang et al., 2017). However, in recent years, with the increasing influence of global climate change and human

47 activities, as well as the uneven distribution of regional water resources, water conservation units such as glaciers,

48 permafrost and grasslands have experienced significant changes, extremely meteorological and hydrological events such as

49 rainstorm, blizzard, droughts and floods have occurred frequently, the spatiotemporal distribution of precipitation and

50 hydrological uncertainties of watersheds have also increased. The sustainable development of ecological environment and

51 social economy over the SRYR is confronted with great challenges (Milly et al., 2002; Yuan et al., 2018).

52 With the rapid development of high-resolution Earth System Models, the role of land surface variability on simulation results

53 is more and more emphasized (Clark et al., 2015; Tang et al., 2019). Currently, most researches on fully coupled

54 atmosphere-hydrology process use regional climate models (RCMs) or land surface models (LSMs) combined with

55 hydrological models to investigate the relationship between climate change and hydrological cycle processes (Kruk et al.,

56 2012). The main technical tools applied include satellite remote sensing, data assimilation, error correction, downscaling

57 (statistical downscaling and dynamic downscaling) analysis. The main models employed are the Weather Research and

58 Forecasting Model (WRF), Community Land Model (CLM), Community Noah Land Surface Model with Multi-

59 Parameterization Options (Noah-MP), and Soil and Water Assessment Tool (SWAT), with a focus on the impact of climate

60 change and human activities on hydrological cycle processes (Cuo et al., 2013; Sheng et al., 2017; Zheng et al., 2018).

61 However, most studies focus on the influence of climate change on the hydrological processes in watersheds, and adopt a

62 single-directional linkage of "atmospheric circulation change-regional precipitation change-land hydrological change",

63 which cannot accurately describe the feedback of land surface and hydrological processes on the regional climate and affect

64 the simulation accuracy of the hydrological processes in watersheds (Wen et al., 2011).

65 The Weather Research and Forecasting Model Hydrological modeling system (WRF-Hydro) is a high-resolution distributed

66 land-atmosphere coupled model developed by the National Center for Atmospheric Research (NCAR) to improve the

67 redistribution of surface, subsurface and river water and to facilitate the coupling of atmospheric and hydrological models

68 (Gochis et al., 2020). The WRF-Hydro model is able to be run either as a standalone land surface hydrological model or

69 coupled with an atmospheric model (such as WRF) to achieve a two-way feedback process between the atmosphere and land

70 surface. Compared to traditional land surface hydrological models, the WRF-Hydro model is designed to provide continuous

71 spatially gridded information on soil temperature and moisture, evapotranspiration, water and heat exchange fluxes, and

72 runoff (Gharamti et al., 2021; Gu et al., 2021). Presently, the WRF-Hydro model has been successfully applied to many

73 fully coupled atmosphere-hydrology studies (Zhang et al., 2019; Fersch et al., 2020; Eidhammer et al., 2021). Senatore et al.

74 (2015) found that the precipitation, surface runoff and surface fluxes simulated by the fully coupled WRF-Hydro model are

75 better than WRF model in the Crati River Basin. Li et al. (2021) concluded that the coupled WRF-Hydro model improved

76 the simulation results of soil moisture and precipitation, and has some potential in simulating and projecting of streamflow

77 over the Source Region of the Three River.

78 The above studies indicate that WRF-Hydro model has a wide range of applications and a strong capability in streamflow

79 simulation, so it has a great potential in climate and hydrology coupled simulation over the SRYR with complex underlying

80 surface conditions. In this research, the fully coupled WRF-Hydro model is used to simulate the rainy season (May-August)

81 of the Yellow River Source basin in 2013, and simulation results are compared to those of the standalone WRF model. The

82 focus is on the analysis of the differences caused by WRF and fully coupled WRF-Hydro for several variables directly

83 related to terrestrial water cycle processes, especially the effects of these variables on precipitation. Materials and

84 methodology are arranged in the section 2 and 3 respectively. The comparison between the simulation performance of the

85 standalone WRF and the coupled WRF-Hydro are followed. And then, the characteristics of fully coupled streamflow are

86 analyzed. Finally, the discussion and main conclusions are provided in section 5 and section 6.

2 Study area and data

2.1 Study area

89 The SRYR (32.12°-35.48°N, 95.50°-103.28°E) lies in the northeast of the TP, with the total catchment area and mean

90 elevation being $1.22×10^5$ km2 and 4000.0 m respectively, as displayed in Fig. 1. This also constitutes the setup of the WRF

91 and fully coupled WRF-Hydro nested domain. The region is located in the edge area affected by the East Asian monsoon

92 and belongs to the plateau cold climate zone with an annual-mean temperature close to 0.0 ℃ and the annual-mean

93 precipitation between 300.0 and 500.0 mm (Ji et al., 2020). As the main flow-producing area and water-conserving area in

94 the middle and upper reaches of the Yellow River, the SRYR is known as the "Yellow River Water Tower", taking the

95 Tangnaihai hydrological station as the outlet of the basin (Zheng et al., 2007). It is mainly composed of high mountains,

96 plains and hills, and is distributed with vast lakes, including the largest plateau fresh water lakes in China, namely the

97   Zhaling Lake and the Eling Lake (Wen et al., 2011). The terrain is undulating with a relatively poor capacity for water

98   holding on the surface, and the main land use type is alpine meadow grassland and alpine wetland. Under the influence of

99   hydrological environment, the soil types are mainly composed of loam and sandy loam with rough texture, and the seasonal

100   frozen soil is widely distributed.
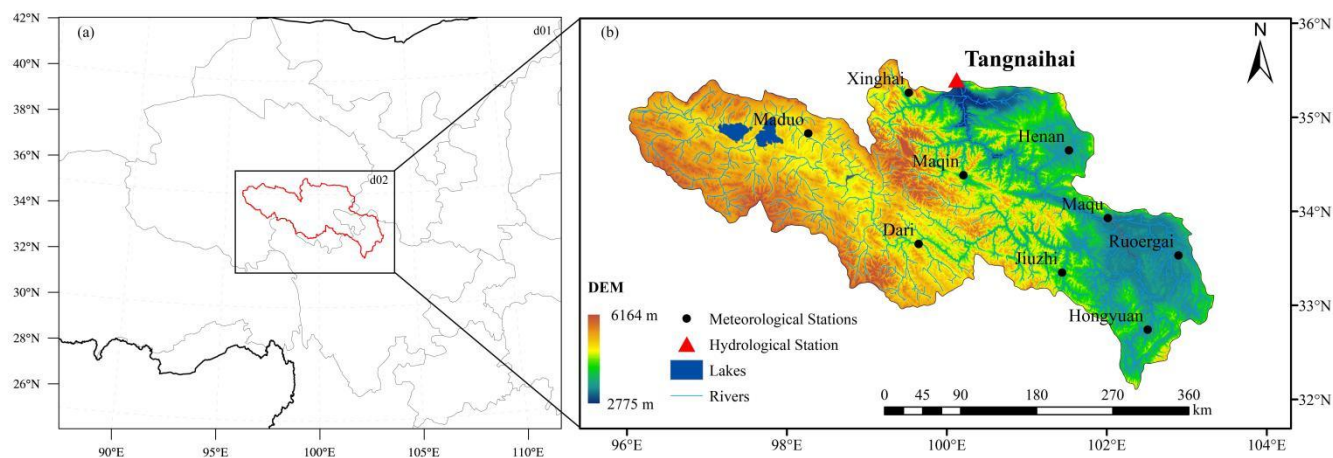
Figure 1. The WRF and WRF-Hydro nested domain (a), and the geographic locations of the meteorological and hydrological stations of the studied catchments (b).

2.2 Data

The daily streamflow data of Tangnaihai hydrological station provided by Yellow River Water Conservancy Bureau during 2012-2013 are employed in this research. Besides, the turbulent heat fluxes and top-layer soil temperature and moisture data of the Eling Lake station (Meng and Lyu, 2022) and Maqu station (An et al., 2019; 2020) from the National Cryosphere Desert Data Center (http://www.ncdc.ac.cn) and the observations of 9 meteorological stations over the SRYR (Fig. 1b) collected from the National Meteorological Information Center of China are also applied.

WRF-Hydro model requires a lot of input data, including meteorological driving data, underlying surface data and river network data. The meteorological driving data are mainly composed of seven variables: downward longwave and shortwave radiation, surface pressure, specific humidity, air temperature, near surface wind speed and precipitation rate. As the SRYR is located in the hinterland of the TP, the meteorological observation stations are rare and unevenly distributed, which brings great difficulties in driving model. The Global Land Data Assimilation System (GLDAS) data are jointly developed by National Aeronautics and Space Administration (NASA) and the National Center of Environmental Prediction (NCEP) with a temporal resolution of three hours and a spatial resolution of $0.25°\times 0.25°$, which integrate the ground and satellite observation data and have great applicability over the SRYR (Li et al., 2014).

In addition, the quality of precipitation data is critical to streamflow simulation and is the most sensitive factor affecting the variation of streamflow, so selecting a high-quality precipitation product as the precipitation driving field of WRF Hydro model is of great significance. The China Meteorological Forcing Dataset (CMFD) is a high spatial-temporal resolution

Hydrology and
Earth System
Sciences
Discussions
Open Access
EGU

121 (0.10°×0.10°) gridded meteorological driving dataset, which is developed for studies of land surface processes in China (He

122 et al., 2020). The dataset integrates a variety of reanalysis, satellite remote sensing and station observation data, and is

123 widely used in climate change and numerical simulations. The CMFD precipitation data combined with GLDAS non

124 precipitation field constitute the final driving data of the model through bilinear interpolation.

125 The initial and boundary conditions for WRF and fully coupled WRF-Hydro model are the Final Operational Global

126 Analysis (FNL), whose spatial and temporal resolutions are 6 h and $1.00° × 1.00°$ respectively

127 (https://doi.org/10.5065/D6M043C6. Accessed 23 Nov 2022). The vegetation type, land use type, soil type and other land

128 surface information required by the model are all from the WPS system, and the default soil type is replaced by the soil type

129 dataset of Beijing Normal University, which has higher accuracy in China. The high-resolution river network data are from

130 the United States Geological Survey (USGS) Hydrological data and maps based on SHuttle Elevation Derivatives at multiple

131 Scales (HydroSHEDS) and the resolution of 90.0 m is selected to extract accurate river network information. The details of

132 the above data are shown in Table 1.

133 **Table 1.** The overview of the research data.

Category	Data Type	Spatial/Temporal resolution	Variables
Climate	CMA (V3.0)	1 d	Precipitation, Temperature,
Hydrology	Site	1 d	Streamflow
Eddy Covariance	Site	30 min	Water/Heat flux, Soil temperature/moisture
	CMFD	3 h; 0.10°×0.10°	Precipitation
Driving Data	GLDAS	3 h; 0.25°×0.25°	Temperature, Wind speed, Solar radiation, Pressure, Specific humidity
	FNL	6 h; 1.00°×1.00°	Initial and boundary conditions
Topography	HydroSHEDS	90.0 m×90.0 m	Digital Elevation Model

134 3 Methodology

135 3.1 Study area

136 3.1.1 WRF model

137 The WRF is an advanced and non-hydrostatic mesoscale numerical weather prediction model, which has ability to meet most
138 mesoscale and small-scale atmospheric and hydrological processes numerical simulation research (Skamarock et al., 2008).
139 The WRF-ARW model (version 4.1.2) is used for both the WRF and fully coupled WRF-Hydro model in this research.

140 3.1.2 Noah-MP model

141 The Noah-MP model was developed from the Noah LSM with several major improvements (Niu et al., 2011; Yang et al.,
142 2011). It provides multiple parameterization options for the key biogeophysical processes, including a separate vegetation
143 canopy, a two-stream radiation transfer approach and a short-term dynamic vegetation scheme. Besides, the frozen soil
144 scheme for the groundwater model and the snow model was also updated, which have significant impact on streamflow
145 simulation (Niu and Yang, 2006). Noah-MP model is selected as the land surface process module of the WRF and the WRF-
146 Hydro model in this research.

147 3.1.3 WRF-Hydro model

148 The WRF-Hydro model, developed as a hydrological extension package for WRF, is a new generation of distributed
149 hydrometeorological forecasting system with physical basis, multi-scale and multi-parameter schemes. It takes the LSM
150 (Noah/Noah- MP) as a bridge, which connects the large-scale regional climate model with the refined hydrological model.
151 The model improves the land surface hydrological process related to the spatial redistribution of land surface water,
152 groundwater and river water, and has capability in quantitatively studying the water-heat exchange process between the
153 atmosphere and land surface (Gochis et al., 2020). The WRF-Hydro model mainly includes five modules, namely surface
154 overland flow, saturated subsurface flow, channel, reservoir routing and conceptual baseflow module. The process of
155 subsurface flow calculates a quasi-3D flow, which takes the vertical and horizontal water exchange into account. The WRF-
156 Hydro system version 5.1.1 is applied in this research and the complete description of the model is available in Gochis et al.
157 (2020).

158 3.2 Experimental designs

159 3.2.1 The parameterization schemes of the WRF and coupled WRF-Hydro model

160 The Lambert Projection is adopted in the model with the central longitude and latitude of 99.50°E and 33.75°N and a two-
161 way nested domains are considered, whose horizontal resolutions of are 25 km and 5 km respectively, as displayed in Fig. 1a.
162 The vertical structure of both domains consists of 40 levels, up to a 50 hPa pressure top with a time step of 100 s in the outer

163 domain. The initial and lateral atmospheric boundary conditions for continuous runs are given by the FNL data (in table 1)
164 which are provided by National Centers for Environment Prediction (NCEP). The physics parameterization schemes
165 employed in this research for the selected WRF domains are listed in the Table 2, in which the cumulus parameterization is
166 only used in the outer domain (Senatore et al., 2015). It is important to note that the routing processes with a resolution of
167 500.0 m are only executed on the innermost domain in the fully coupled WRF-Hydro model. The simulation starts from
168 March 1st, 2013 to September 1st, 2013 UTC with the first two months as the spin-up time and the rest for analysis.

169 **Table 2.** Physical options of WRF and the fully coupled WRF-Hydro model.

Physics process	Parameterization	Reference
Microphysics	Thompson	Thompson et al. (2008)
Cumulus parameterization	Grell-Devenyi (GD)	Grell and Devenyi (2002)
Planetary boundary layer	MYNN2	Nakanishi and Niino (2006)
Land surface	Noah-MP	Niu et al. (2011)
Longwave radiation	RRTMG	Iacono et al. (2008)
Shortwave radiation	RRTMG	Iacono et al. (2008)

170 **3.2.2 The parameterization schemes of the WRF and coupled WRF-Hydro model**

171 Before analyzing the effects of the land-hydrological processes on the atmosphere simulation, WRF-Hydro model is run in
172 an offline/uncoupled way with the aim of calibrating relevant sensitive parameters and evaluating the performance of the
173 model in simulating streamflow.

174 The parameters of the hydrological models are able to reflect the underlying surface characteristics of the region and there
175 are significant discrepancies in the applicability of the default parameters in models over different basins. In terms of the
176 WRF-Hydro model, most studies have divided the sensitivity parameters for controlling streamflow process into those for
177 controlling streamflow distribution and water volume and those for controlling flood peak and flood hydrograph (Gu et al.,
178 2021). A stepwise manual approach is adopted in calibrating the sensitive parameters, following previous WRF-Hydro
179 studies (Yucel et al., 2015). It is important to note that the slope of the SRYR is steep, which is different from that of the
180 Daihe River Basin (Wang et al., 2021). Therefore, the surface retention depth (RETDEPRTFAC) is set as 0.0, and only four
181 parameters listed in Table 3 are to be calibrated.

182

183

184

185

186

187

188 **Table 3.** The sensitive parameters of streamflow formation in WRF-Hydro model.

Classification	Parameter name	Default	Range
Water volume	SMCMAX	-	0.6~1.2 times
	REFKDT	3.0	0.1~5.0
Hydrograph	MannN	-	0.3~2.0 times
	OVROUGHRT	1.0	0.0~1.0

189

190 Additionally, the water-heat exchange process is of vital importance to the understanding on the atmosphere-land-hydrology

191 process, which has ability to affect the land-surface water cycle process by influencing the evapotranspiration process.

192 Relevant studies show that the default parameterization schemes of Noah-MP model underestimated latent heat (LE) and

193 overestimated sensible heat (H) over the alpine grassland area (Ye et al., 2017). The Chen97 scheme for sensible heat

194 transfer coefficient is able to overcome the problem on overestimating H, while the Jarvis canopy stomatal resistance scheme

195 effectively increases the transpiration of vegetation, so as to improve the simulated LE, and make the distribution of heat

196 flux between LE and H more reasonable. Table 4 shows the parameterization options of Noah-MP used in this research.

197 **Table 4.** Parameterization scheme options of Noah-MP used in this research.

Physical Process	Option
Dynamic vegetation	Use table LAI; use maximum vegetation fraction
Canopy stomatal resistance	Jarvis
Soil moisture factor for stomatal resistance	Noah
Runoff and groundwater	Original surface and subsurface runoff
Surface layer drag coefficient	Chen97
Supercooled liquid water	No iteration
Frozen soil permeability	Linear effects, more permeable
Radiation transfer	Two-stream applied to vegetated fraction
Snow surface albedo	CLASS
Rainfall and snowfall	Jordan
Lower boundary of soil temperature	Original Noah
Snow and soil temperature	Semi-implicit, but FSNO for TS calculation
Surface resistent to evaporation/sublimation	Sakaguchi and Zeng for non-snow, rsurf = rsurf_snow for snow
Glacier treatment	Slab ice

Hydrology and
Earth System
Sciences
Discussions

3.3 Evaluation index

In order to evaluate the model performance of the simulations, Nash Efficiency Coefficient (NSE), Root Mean Square Error (RMSE), Correlation Coefficient (R) and Relative Deviation (BIAS) are selected in this research. The calculation formula and optimal value of each evaluation index are shown in Table 5.

Table 5. The evaluation indices for simulation performance.

Indices	Calculation formula	Optimal value
Correlation Coefficient	$R = \sum_{i=1}^{N} (S_i - \bar{S})(O_i - \bar{O}) / \sqrt{\sum_{i=1}^{N} (S_i - \bar{S})^2 \sum_{i=1}^{N} (O_i - \bar{O})^2}$	1
Root Mean Square Error	$RMSE = \sqrt{\sum_{i=1}^{N} (S_i - O_i)^2 / N}$	0
Nash Efficiency Coefficient	$NSE = 1 - \sum_{i=1}^{N} (S_i - O_i)^2 / \sum_{i=1}^{N} (O_i - \bar{O})^2$	1
Relative Deviation	$BIAS = \sum_{i=1}^{N} (S_i - O_i) / \sum_{i=1}^{N} O_i \times 100\%$	0

where N is the number of samples, S_i and O_i represent simulated and observed values respectively.

3.4 Analysis on the applicability of the WRF-Hydro model

After 2 months spin-up time, the uncoupled WRF-Hydro is calibrated for the period from 1st, June to 1st, September in 2012 based on daily streamflow in Tangnaihai hydrological station. Fig. 2 exhibits that the simulated streamflow is close to the observation, and the flood hydrograph is consistent with the precipitation hydrograph. For the calibration period, the R of simulated and measured streamflow is 0.84, the NSE is 0.44, the RMSE is 465.61 m^3·s^{-1}, and the BIAS is -11.44%. For the validation period, The R is 0.81, the NSE is 0.61, the RMSE is 351.36 m^3·s^{-1}, and the BIAS is -10.21%. However, the simulated streamflow underestimates the peak flow in flood season and presents some unrealistic peak flows which suggests the oversimplified base flow model and the uncertainty of the forcing precipitation (Senatore et al., 2015). Nevertheless, the WRF-Hydro model has ability to produce realistic hydrological regime over the SRYR. Therefore, the calibrated parameters are used in the comparison between the WRF and the fully coupled WRF-Hydro simulations.
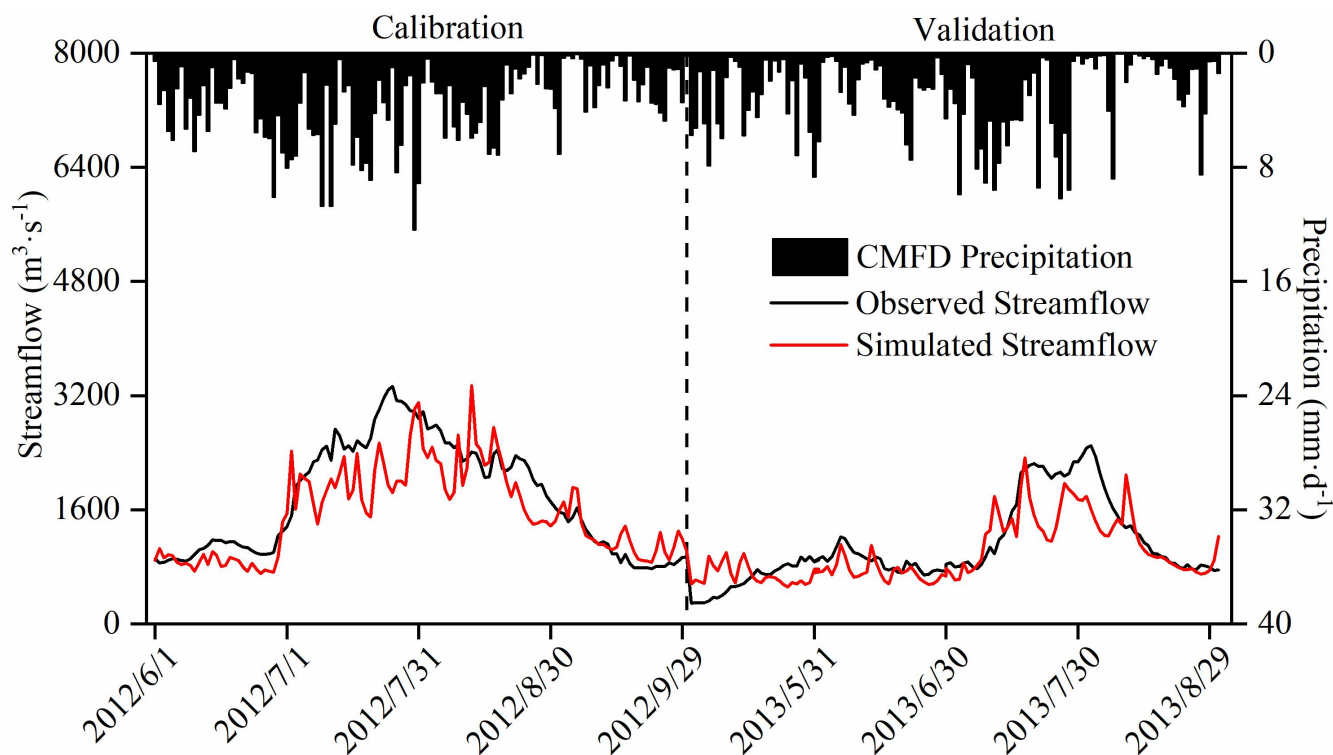
Figure 2. The variation of simulated and observed daily streamflow (units: $m^3 \cdot s^{-1}$) over the Source Region of the Yellow River during the calibration and validation period. Black dotted line in correspondence of September 30th, 2012 splits calibration and validation periods.

Besides, the LE and H fluxes simulated by the uncoupled WRF-Hydro model are also discussed. In order to ensure data comparability, the typical sunny/cloudy days at Eling Lake (lakeside underlying surface) and Maqu (grass underlying surface) stations are selected by characteristic downward total radiation patterns from the entire simulation period. The screening methods of typical sunny/cloudy days are consistent with Zhang et al. (2022).

Fig. 3 and Fig. 4 show the diurnal variation characteristics of LE and H fluxes at two typical flux stations over the SRYR on the typical sunny and cloudy days. On the typical sunny day, the simulated LE is in good agreement with the observation, with the R of 0.92 and 0.96 respectively, and the RMSE of 24.71 $W \cdot m^{-2}$ and 26.89 $W \cdot m^{-2}$. However, there are some differences in the simulation performance of H between the two stations. The WRF-Hydro model has ability to better simulate the diurnal variation of H at the Ealing Lake station with the R of 0.92 and the RMSE of 15.21 $W \cdot m^{-2}$, while underestimates H at Maqu station with the RMSE of 30.29 $W \cdot m^{-2}$.

Due to the complexity of climate conditions on the typical cloudy day, the consistency of simulations and observations is not as good as that on the typical sunny day. On the typical cloudy day, the R between the simulated LE and the observation at two stations is above 0.65 and the RMSE is larger than that of typical sunny days, which is 34.77 $W \cdot m^{-2}$ and 31.30 $W \cdot m^{-2}$, respectively. The simulated H is unable to capture the multi-peak characteristics of H, especially in the Eiling Lake station

233   with the R of 0.37, while the RMSEs are only 23.66 W·m⁻² and 20.25 W·m⁻². Overall, the WRF-Hydro model has ability to

234   represent the water-heat exchange process between land and atmosphere over the SRYR.
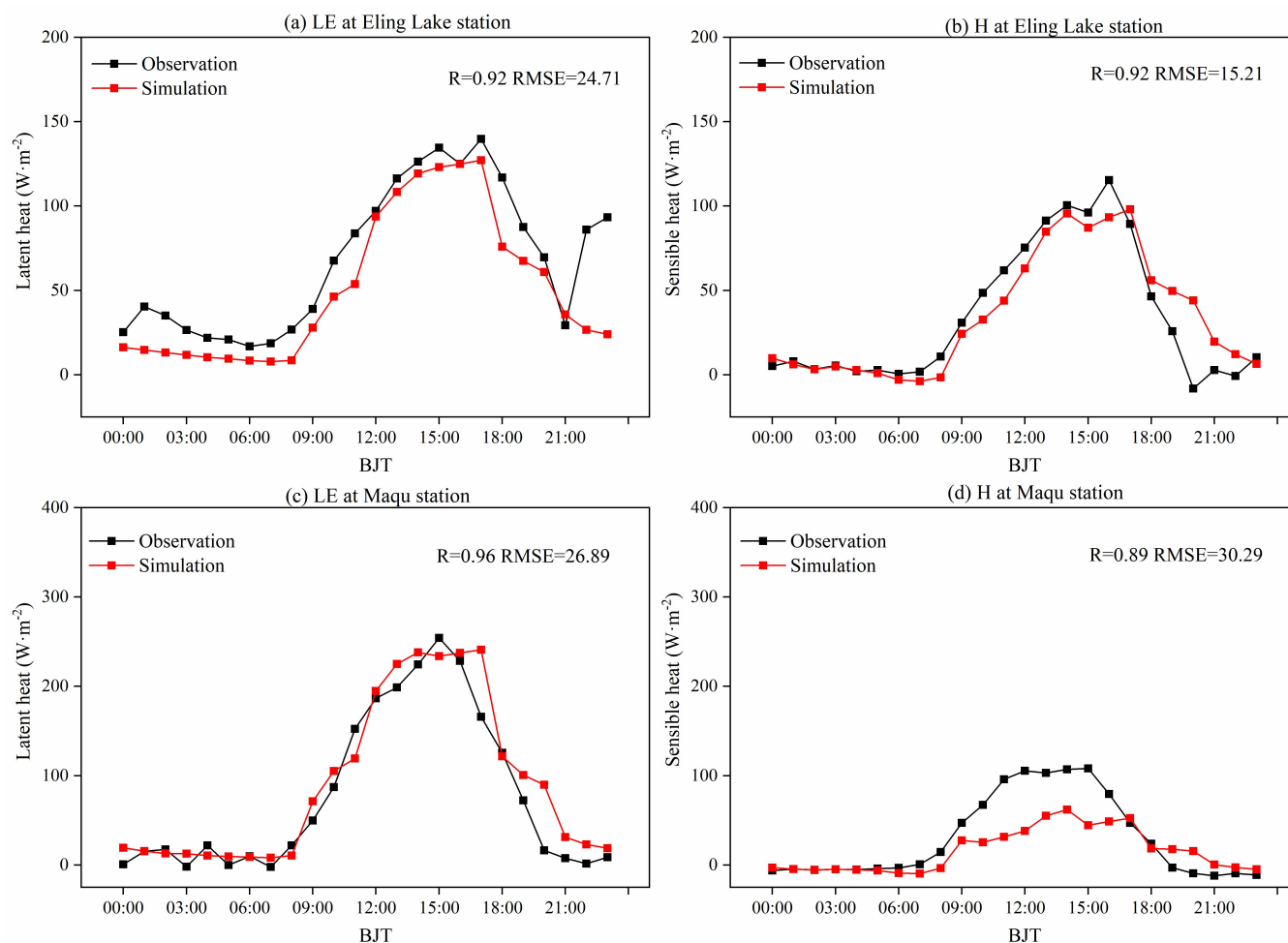
235

236   **Figure 3**. The turbulent fluxes (units: W·m⁻²) simulated by uncoupled WRF-Hydro model on the typical sunny days at Eling

237   Lake (a-b) and Maqu (c-d) station. Where R represents the correlation coefficient and RMSE is the Root Mean Square Error.
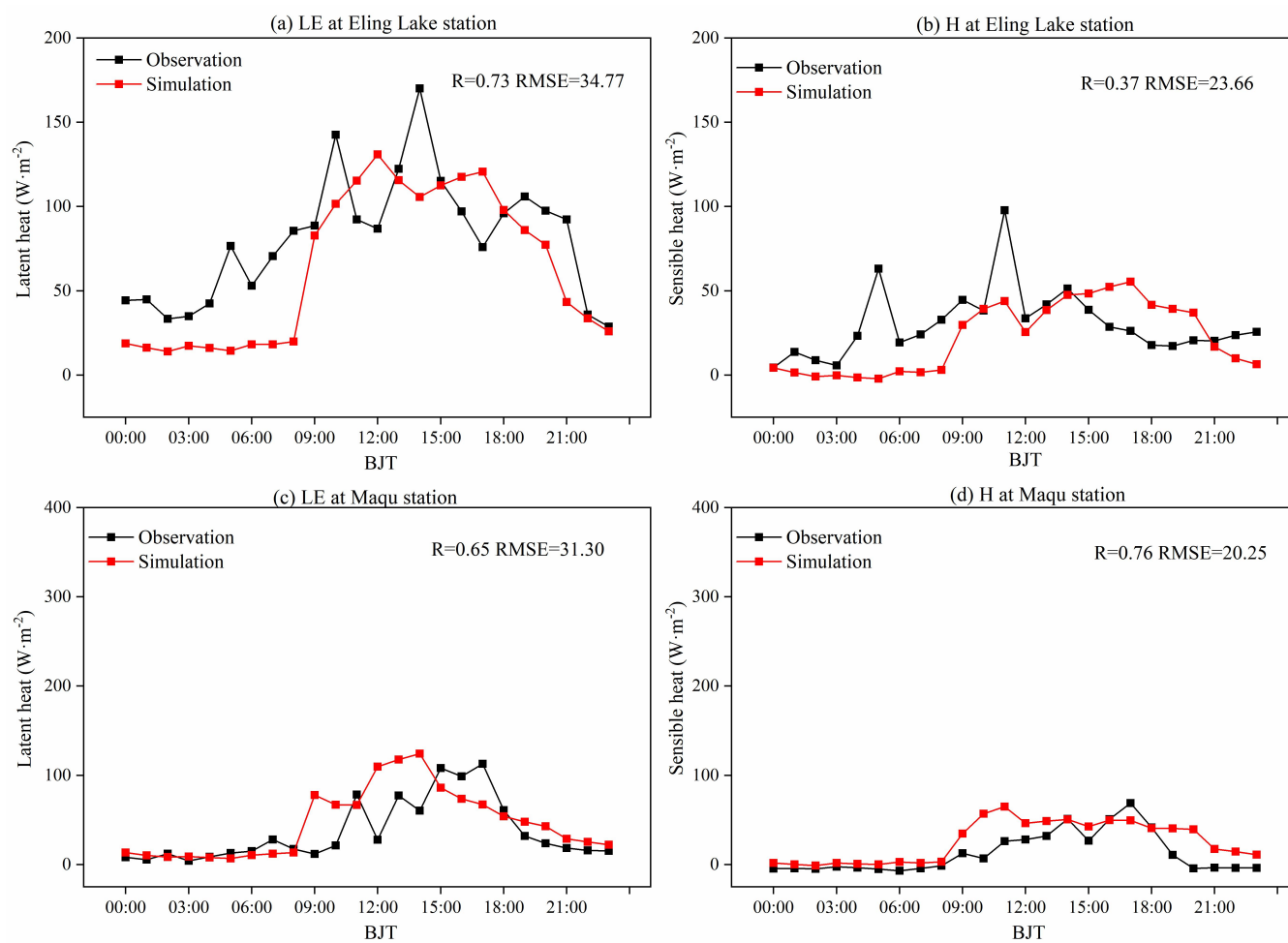
Figure 4. As in Figure 3, but for the typical cloudy days.

4 Results

Land surface hydrological cycle is one of the important processes in the Earth System. On the one hand, climate change drives the water cycle process at the global scale and causes different responses at the regional scale. On the other hand, the variations of land surface process further alter the distribution of water resources and runoff at regional and catchment scales (Meng et al., 2020). Based on the fully coupled WRF-Hydro model, the impact of climate change on land surface hydrological processes and the feedback of surface water cycle to precipitation are comprehensively considered, and the variation characteristics of the coupled process of atmosphere-land-hydrology and streamflow over the SRYR in the rainy season (May-August) of 2013 are also explored.

4.1 The validation of temporal variation of hydrometeorological elements

The influence of global climate change on hydrological environment is extremely significant, in which temperature and precipitation are the key factors to the redistribution of water cycle in time and space (Meng et al., 2020). Precipitation directly participates in all aspects of the water cycle, while temperature also indirectly influences the whole process of the water cycle through evaporation and snowfall. Therefore, the simulation performance is first evaluated by comparing precipitation and temperature from WRF and coupled WRF-Hydro simulations with observations.

Fig. 5 exhibits the Taylor diagrams (Taylor, 2001) for daily precipitation and temperature among simulations with observations of 9 meteorological stations. The simulated precipitation is in good agreement with the observations, with the correlation coefficients higher than 0.6. The standardized deviation ratios of the coupled WRF-Hydro to the observations are between 0.8 and 1.2 with greater RMSE than the standalone WRF model, which means that the coupled process increases the wet bias of precipitation simulation since considering the terrestrial lateral flow of soil water. In terms of temperature, both two experiments perform well in simulating temperature, with the average R is 0.93 and a slight cold deviation.
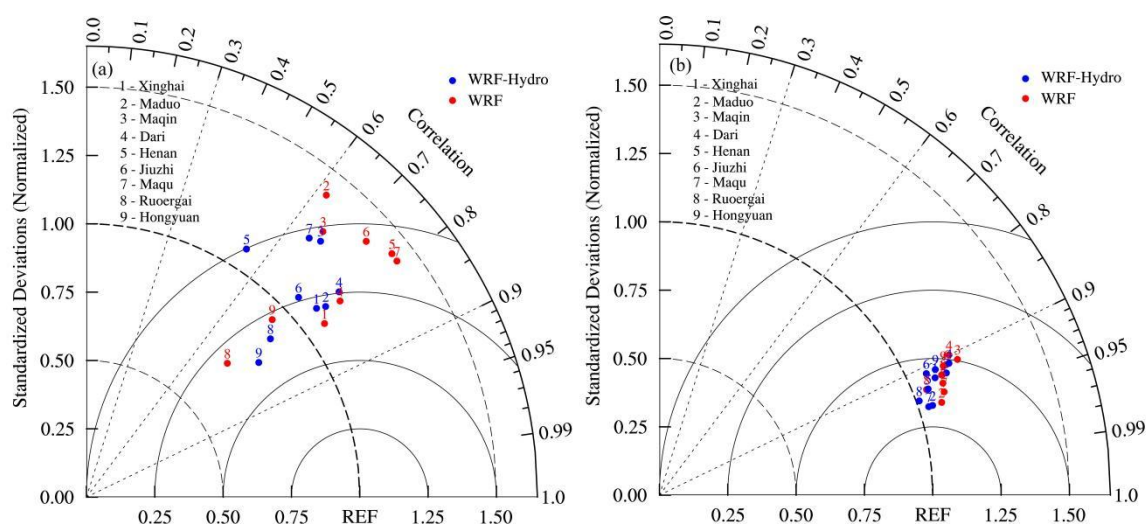
Figure 5. Taylor diagrams of correlation coefficients and standard deviations for daily precipitation and temperature over the SRYR among simulations with observations from May 1st, 2013 to August 31st, 2013.

Since the sparse and uneven distribution of stations over the SRYR, the reanalysis products are employed to analyze the spatial variation of the hydrometeorological elements in this research. Relevant researches (Li et al., 2014; Chen et al., 2022) indicate that CMFD precipitation data have good applicability over the SRYR, and climate and hydrological factors such as temperature and runoff of GLDAS have ability to better characterize the climate change and water cycle processes over the SRYR. Therefore, CMFD and GLDAS are taken as reference (denoted as Reference) datasets to compare and analyze the regional mean simulation results in the following study.

269　Fig. 6 shows that the time series of regional mean meteorological and hydrological elements. It exhibits that both WRF and
270　fully coupled WRF-Hydro model are able to characterize the evolution characteristics of meteorological and hydrological
271　elements over the SRYR. Compared with standalone WRF model, the coupling process slightly increases the wet deviation
272　of precipitation, while it improves the simulation of temperature and downward longwave and shortwave radiation to a
273　certain extent. The simulations of surface pressure, specific humidity of 2m and wind speed near the ground have little
274　difference in two experiments. However, the coupling process increases soil moisture due to considering of the terrestrial
275　vertical and lateral flow of soil water in three-dimensional space, so the simulation results of evapotranspiration are larger.

276

Hydrology and
Earth System
Sciences
Open Access
Discussions
EGU
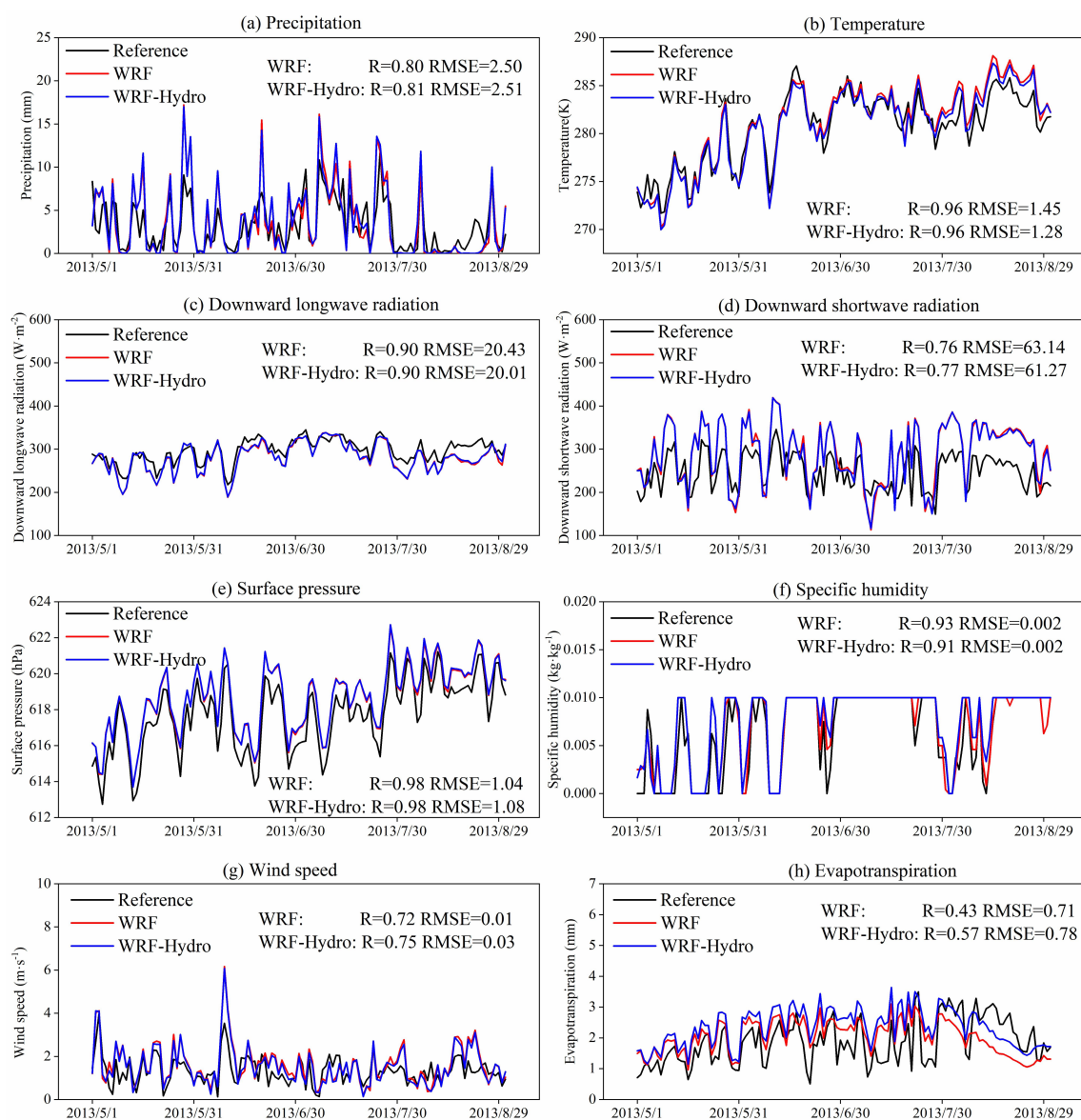
277 **Figure 6**. The time series of mean meteorological and hydrological elements simulated by WRF and fully coupled WRF-
278 Hydro model from the period of May 1st, 2013 to August 31st, 2013.

279 The land-atmosphere water and heat exchange processes affect the surface soil moisture by changing evapotranspiration and
280 further impacts the surface energy and hydrological cycle process (Jia et al., 2014). The diurnal variation characteristics of
281 the LE and H simulated by WRF and coupled WRF-Hydro model on the typical sunny days, when the land-atmosphere
282 water and heat exchange process is relatively strong, are analyzed in Fig. 7. The results at Eling Lake station show that the
283 LE and H simulated by fully coupled WRF-Hydro model are more consistent with the measured, with the RMSE reducing to
284 29.91 W·m^{-2} and 31.06 W·m^{-2} compared with WRF simulations. For the Maqu station, the coupled process increases the
285 deviation of LE simulations, which is related to the overestimation of evapotranspiration, while the problem that H are
286 overestimated is greatly improved.
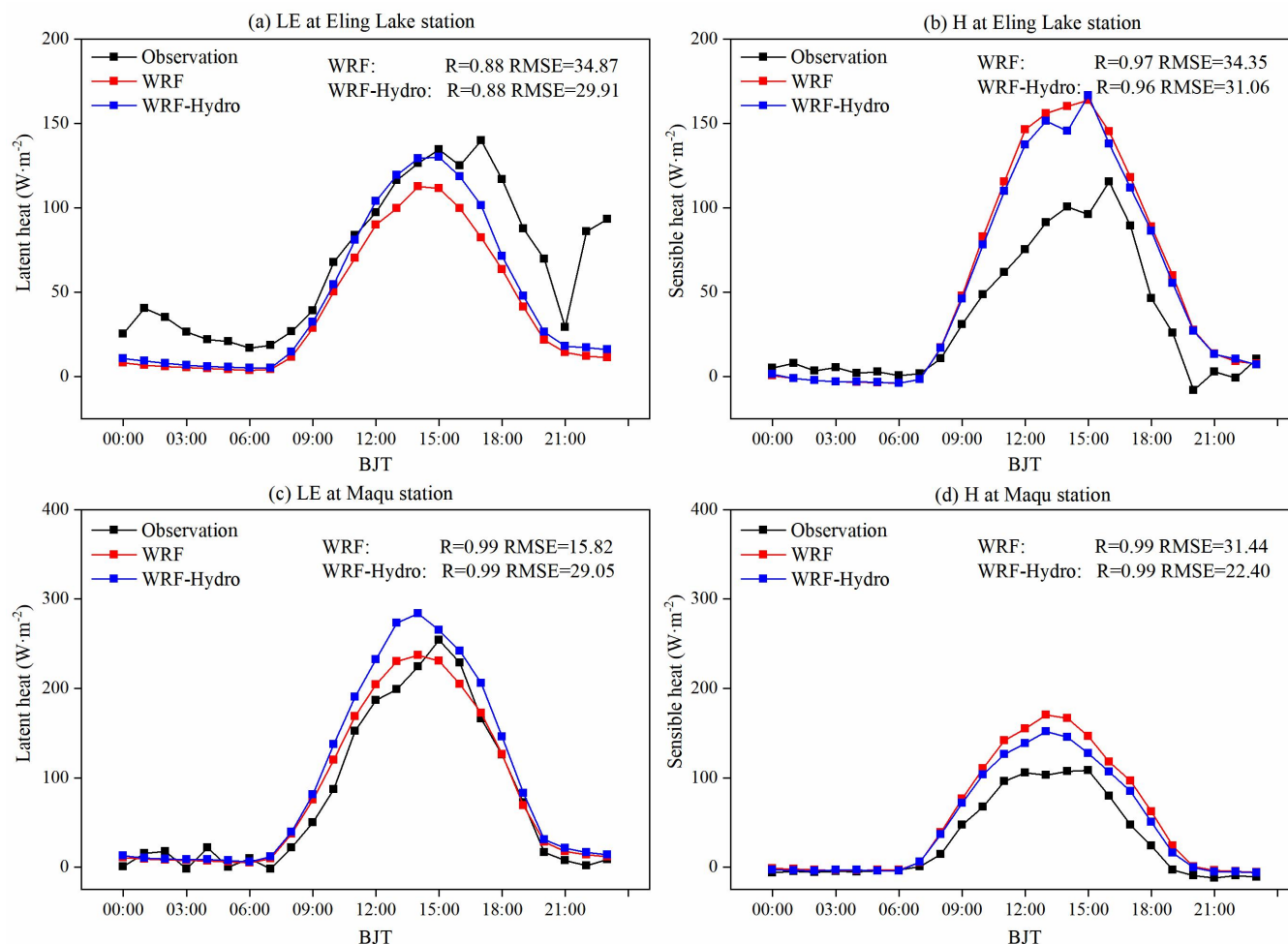
287
288 **Figure 7.** Comparison of turbulent fluxes (units: W·m^{-2}) between WRF-Hydro/ WRF and observations on the typical sunny
289 days at Eling Lake (a-b) and Maqu (c-d) station.

290   Fig. 8 demonstrates the diurnal variation characteristics of the LE and H on the typical cloudy days, when the weather

291   conditions and physics processes are more complicated. On the typical cloudy days, the agreement of the turbulent fluxes

292   simulation results with observations is not as good as that on the typical sunny day. The simulations at two stations indicate

293   that coupled process is able to reduce the RMSE in LE and H with a mean RMSE of 29.48 $W \cdot m^{-2}$ and 26.55 $W \cdot m^{-2}$

294   respectively.

295   Overall, the coupled WRF-Hydro simulations improve the simulation of surface heat flux variables duo to the consideration

296   of the lateral terrestrial water flow of hydrological process.

297

298
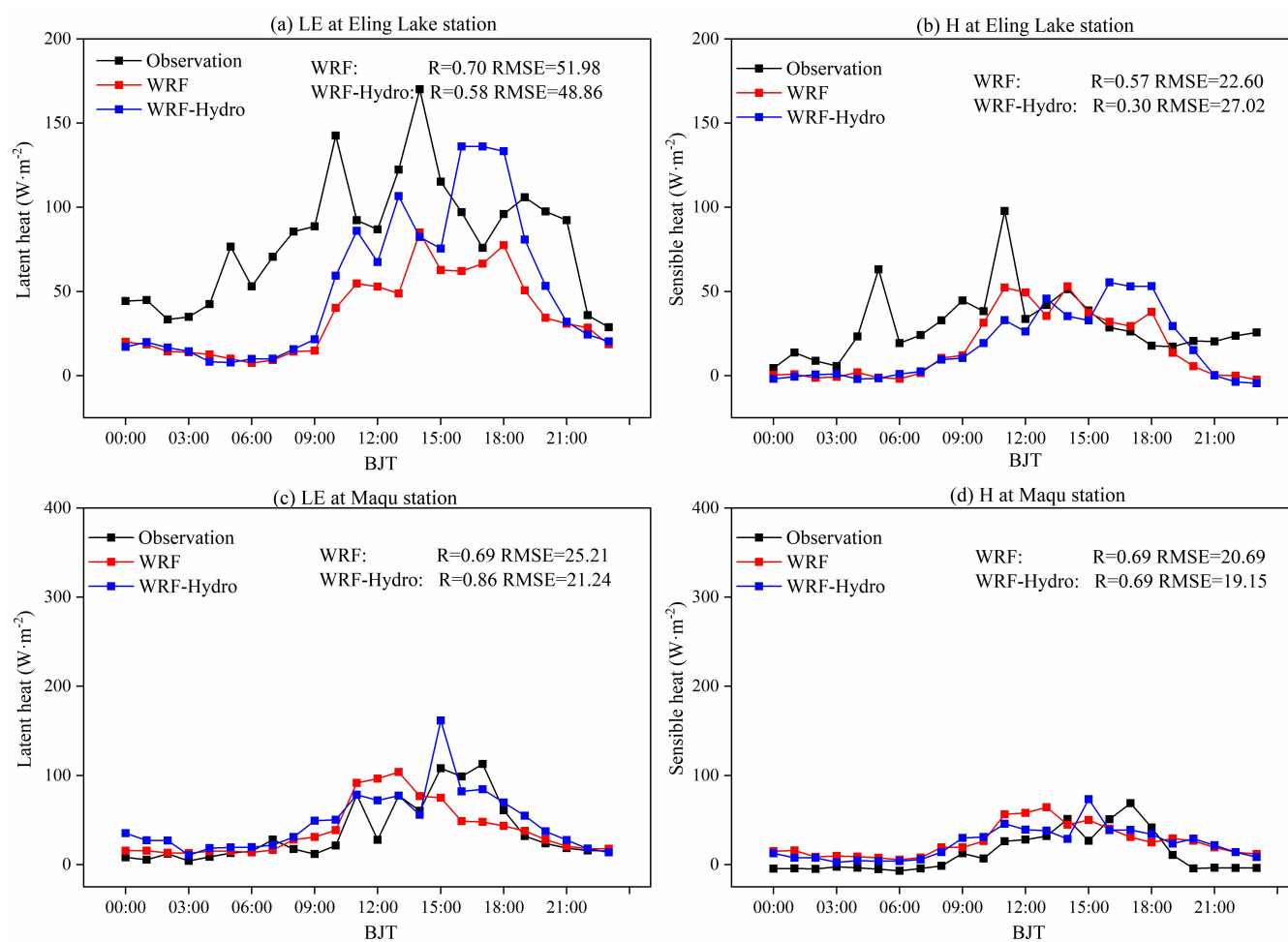
Figure 8. As in Figure 5, but for the typical cloudy days.

300   Soil temperature and moisture are able to affect the land-surface evaporation and groundwater processes, directly or

301   indirectly affect the land-hydrology process. Therefore, the top-layer soil temperature and moisture at Maqu station are

302   analyzed in Fig. 9 due to the availability of observed data. The results display that the soil temperature simulated by WRF

303   and coupled WRF-Hydro model is in good agreement with observation. However, the simulated soil temperature is far
304   greater than the observed in August, which is related to the deviations from the downward shortwave radiation and
305   temperature (Fig. 6). The coupling process reduces the RMSE of soil temperature simulation (from 5.18 to 4.22 K) for the
306   comprehensive consideration in the variation of soil water content. Besides, WRF-Hydro maintains a longer soil moisture
307   memory with respect to the standalone WRF run and the simulated soil moisture values from WRF-Hydro significantly
308   exceed WRF ones (Fig. 9b), which is due to the subsurface lateral flow considered in WRF-Hydro model. The simulated top-
309   layer soil moisture of both experiments is not consistent with the observation and has difficulty in reflecting the response of
310   soil moisture to precipitation. Additionally, the comparison of site results also brings uncertainty to the judgment of
311   simulation performance which needs to be verified in spatial distribution.

312

17
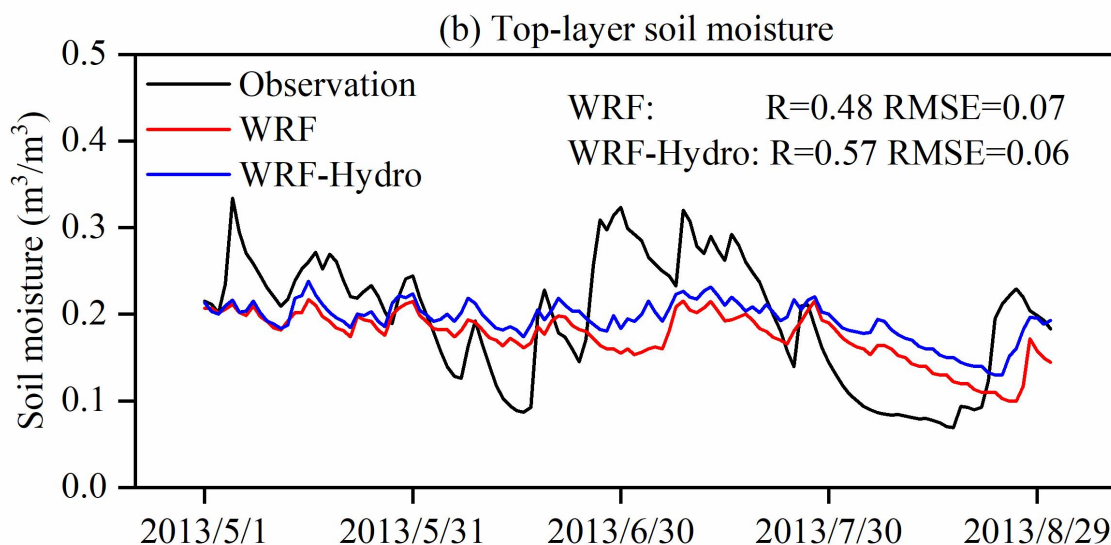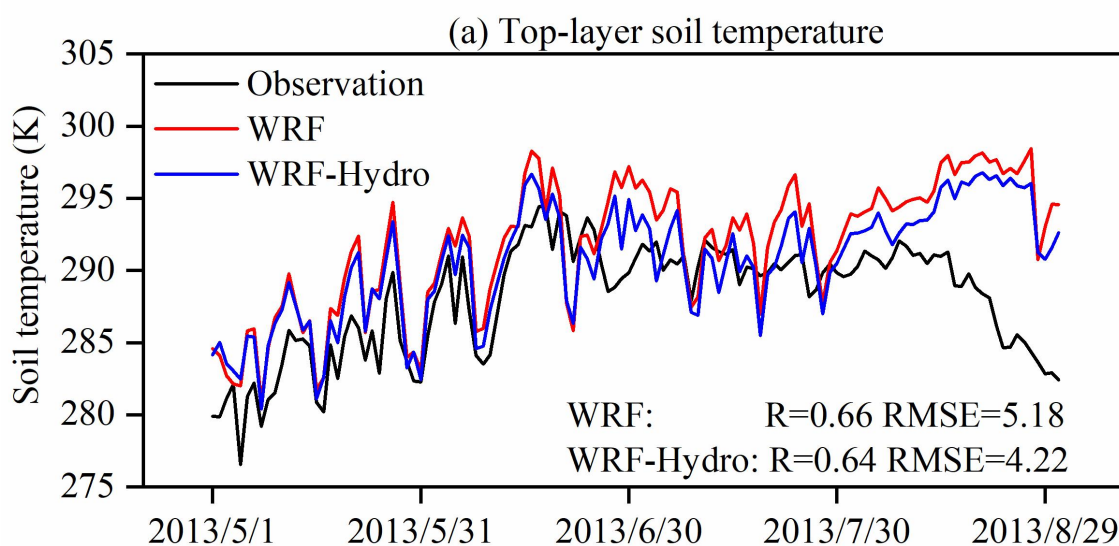
313   **Figure 9.** The time series of top-layer soil temperature (units: K) and moisture (units: m^3/m^3) simulated by WRF and fully
314   coupled WRF-Hydro model from the period of May 1st, 2013 to August 31st, 2013.

4.2 The validation of spatial distribution of hydromteorological elements

316   Furthermore, the spatial distribution of the accumulated precipitation for CMFD reference data (denoted as Reference), WRF
317   and coupled WRF-Hydro, as well as their differences are displayed in Fig. 10. The precipitation highlights the strong
318   dependence of rainfall patterns on topography and shows a decreasing trend from southeast to northwest over the SRYR.
319   The WRF and fully coupled WRF-Hydro have ability to better capture the distribution characteristics of precipitation. The
320   simulations of both experiments have a significantly wet bias, especially in the Jiuzhi and Maqu area, while a dry bias in the
321   southeastern SRYR. Compared with the standalone WRF, the coupled WRF-Hydro takes the subsurface lateral flow into
322   consideration, which leads to the increase of soil moisture and a more reasonable spatial distribution of soil water, so as to
323   have a feedback effect on precipitation with a mean wet bias of 16.63 mm than WRF simulations.

324
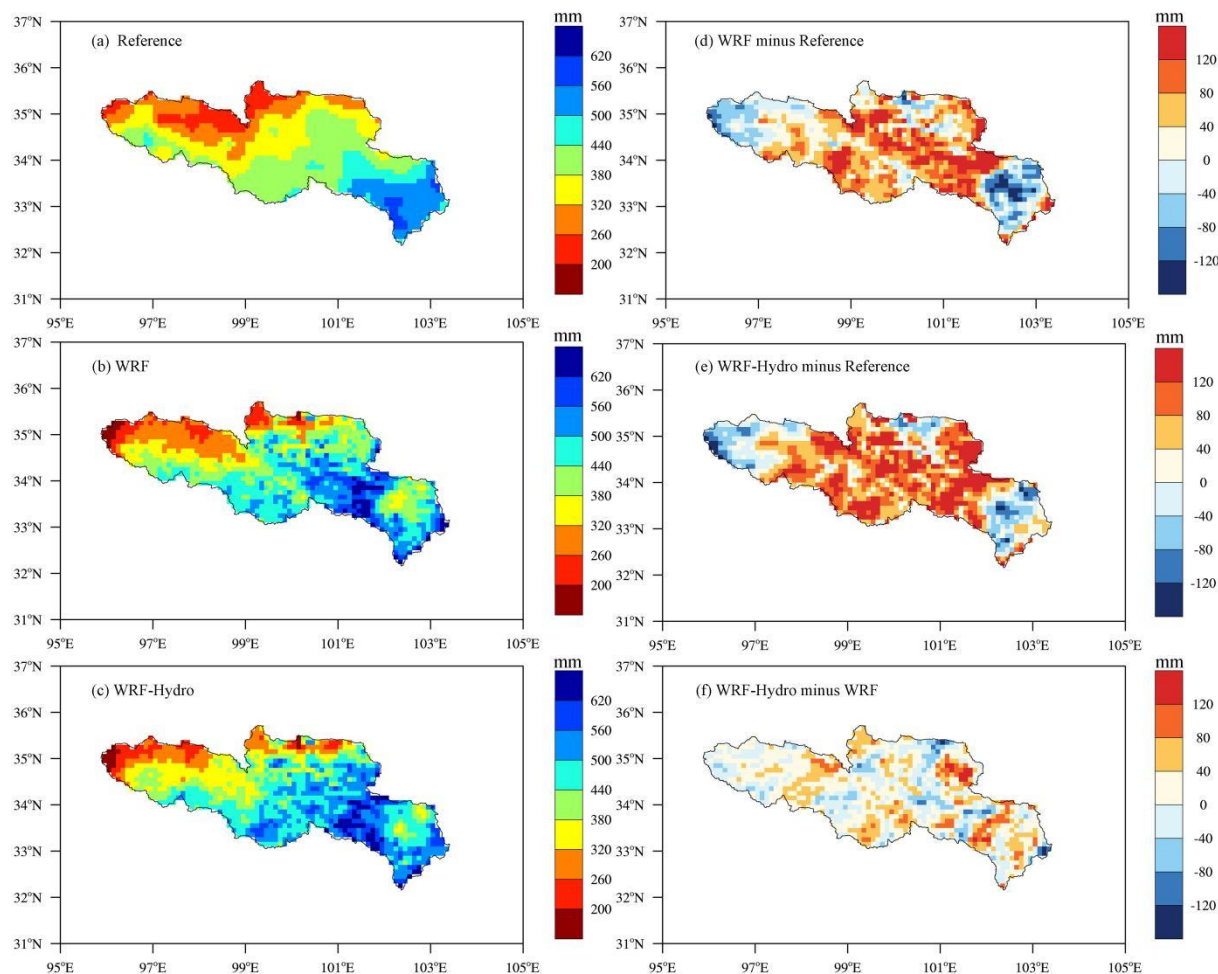
Figure 10. The spatial distribution of the accumulated precipitation (units: mm) in the time interval May 1st, 2013 to August 31st, 2013 with (a) observation, (b) the standalone WRF simulation, (c) the coupled WRF-Hydro simulation, and difference map for (d) WRF minus observation, (e) WRF-Hydro minus observation, (e) WRF-Hydro minus WRF.

With the respect to temperature, the spatial patterns of the mean 2-m air temperature during the simulated period are showed in Fig. 9. The spatial distribution of temperature presents gradient characteristics with higher temperatures in the flat regions and lower temperatures in the alpine areas. Both experiments have ability to capture the distribution characteristics of temperature well. On the whole, the simulated temperature is relatively higher, especially in the northeast of the SRYR, with a regional mean bias of 0.44 K for standalone WRF and of 0.15 K for the fully coupled WRF-Hydro respectively, which means that the coupled simulation slightly reduces the deviation of the mean temperature.
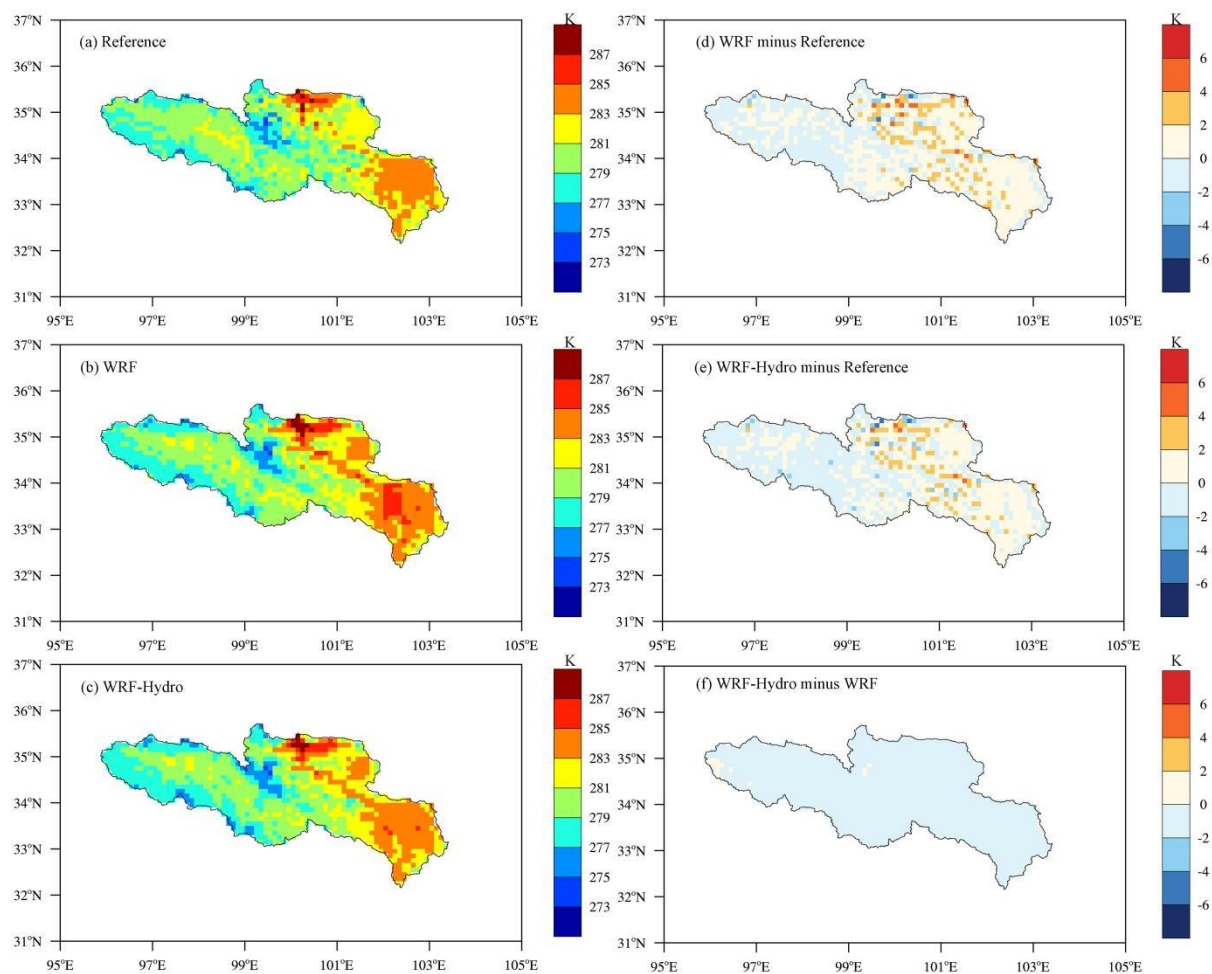
Figure 11. As in Figure 8, but for the mean temperature (units: K).

336 The spatial distribution of turbulent fluxes is able to affect the development of the atmospheric boundary layer through

337 thermal exchanges, and then change the precipitation structure and area (Zhang et al., 2019). Fig. 12 shows the spatial

338 distribution of the LE and H simulated by WRF and coupled WRF-Hydro models and their differences. As far as LE is

339 concerned, both experiments demonstrate a southeast-northwest gradient with two maximum value areas of LE in Zhaling

340 Lake and Eiling Lake, which is related to the evaporation process of lakes. Compared to standalone WRF (mean value 55.89

341 $W \cdot m^{-2}$), the coupled simulation (mean value 68.98 $W \cdot m^{-2}$) increases the LE simulation values due to the increase in

342 evaporable area. In terms of H, its spatial distribution is the opposite of LE, showing decreasing characteristics from

343 northwestern to southeastern SRYR, with a low value area for simulated H in the two lakes. The coupled simulation

344 significantly reduces the simulated H and overcomes the problem of large H simulation, with a mean difference of -4.2

345 $W \cdot m^{-2}$ between the coupled WRF-Hydro and WRF.
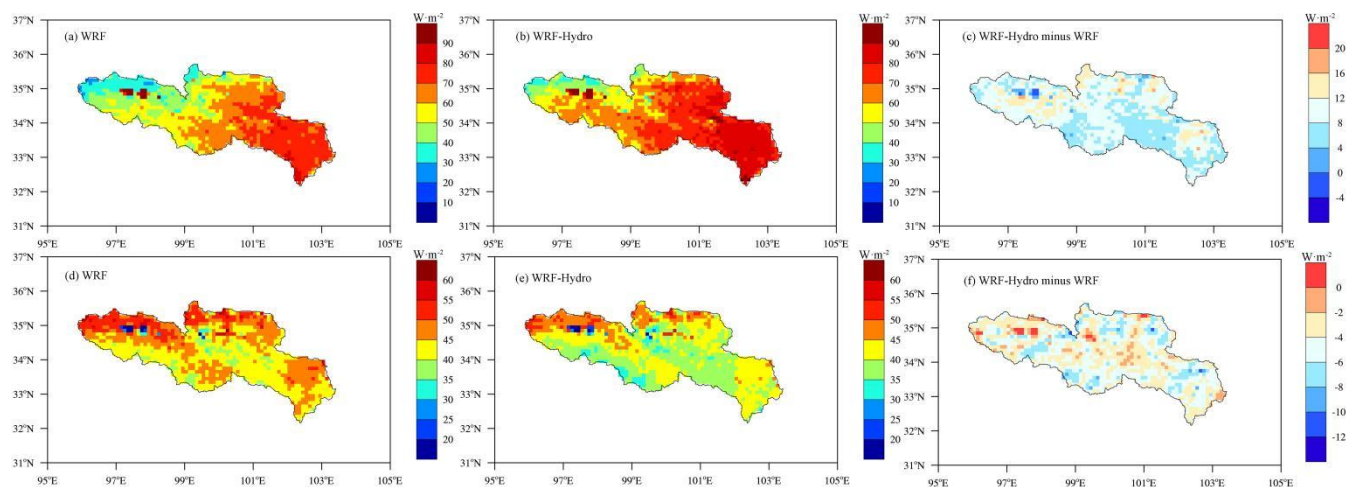
Figure 12. The spatial distribution of the mean latent heat (units: $W \cdot m^{-2}$) in the time interval May 1st, 2013 to August 31st,

348 2013 with (a) the standalone WRF simulation, (b) the coupled WRF-Hydro simulation, and difference map for (c) WRF-

349 Hydro minus WRF, (d-f) are same as (a)-(c), but for sensible heat (units: $W \cdot m^{-2}$).

350 Soil temperature is an important parameter of land surface process, which directly reflects the land thermal state. Its variation

351 affects the movement and phase transition of surface soil water, thus affecting the surface hydrological cycle (Zhang et al.,

352 2021). Soil moisture is a key factor affecting land-atmosphere interaction. As a storage term for heat and moisture, soil

353 moisture has the ability to remembering from weeks to months, remembering previous atmospheric perturbations and then

354 influencing the atmosphere through factors such as surface fluxes (Song et al., 2019).

355 The spatial distribution characteristics of top-layer soil temperature (Fig. 13a, b, c) and moisture (Fig. 13d, e, f) during the

356 2013 rainy season over the SRYR are analyzed in Fig. 13. Due to the high altitude and the large temperature difference

357 between day and night over the TP, its mean temperature is lower than that of the inland areas, so the closer to the depth of

358 the plateau, the lower the soil temperature. Both experiments are able to better depict the characteristic that the temperature

359 in the lake area is lower than the surrounding area, and the coupled WRF-Hydro reduces the simulated surface soil

360 temperature, with a cold deviation of 1.07 K, which is able to affect the atmospheric water vapor convergence through land-

361 atmosphere interactions. For soil moisture, both experiments show that wet centers in the Zaling Lake and Eling Lake area.

362 Influenced by the terrestrial lateral water and soil moisture redistribution process of coupled WRF-Hydro, the spatial

363 distribution of soil water content is more reasonable over the study region, and WRF-Hydro soil moisture values

364 significantly exceed WRF ones, with a wet deviation of 0.02 m^3/m^3. On the whole, the two lakes and the surrounding areas

365 over the SRYR are cold and wet centers during the simulation period, and the coupled simulations better capture the

366 variation characteristics of soil temperature and moisture.

367
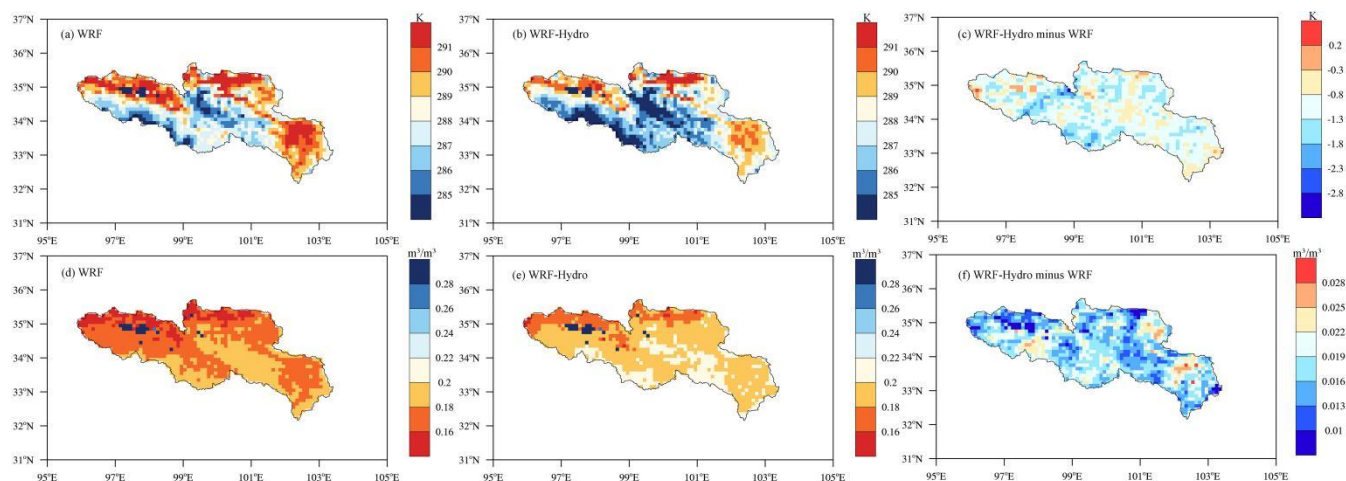
368 **Figure 13.** The spatial distribution of the mean top-layer (0-10 cm) soil temperature (units: K) in the time interval May 1st,

369 2013 to August 31st, 2013 with (a) the standalone WRF simulation, (b) the coupled WRF-Hydro simulation, and difference

370 map for (c) WRF-Hydro minus WRF, (d-f) are same as (a)-(c), but for soil surface temperature (units: m^3/m^3).

371 **4.3 The time series of the streamflow simulated by the fully coupled model**

372 The time series of fully coupled simulated streamflow for the 2013 rainy season when no direct meteorological station

373 observations are required are given in Fig. 14. The fully coupled model is able to capture the temporal variation of observed

374 hydrographs with a R of 0.77. However, reproducing the daily streamflow with the fully coupled model still remains a

375 challenge with a NES of 0.33 and a RMSE of 458.85 $m^3 \cdot s^{-1}$. The main reason is that the coupled simulated streamflow is

376 severely overestimated, especially the reproduction of peak flow is very limited. The performance degradation is mainly due

377 to the fact that the WRF-Hydro model is extremely sensitive to the quality of precipitation data, where the RMSE of

378 precipitation is only 2.51 mm, but the RMSE of streamflow reaches 458.85 $m^3 \cdot s^{-1}$. Besides, this error may also be due to the

379 different frequencies of the Noah-MP LSM called in the uncoupled calibration and fully coupled runs. During the uncoupled
380 simulations, the Noah-MP LSM is typically invoked at the physical time step of the hydrological model, whereas during
381 fully coupled simulations, it is invoked at the physical time step of the WRF model, which results in more water passing
382 farther downslope or into the channel before infiltration occurs again, implying higher streamflow values (Senatore et al.,
383 2015).
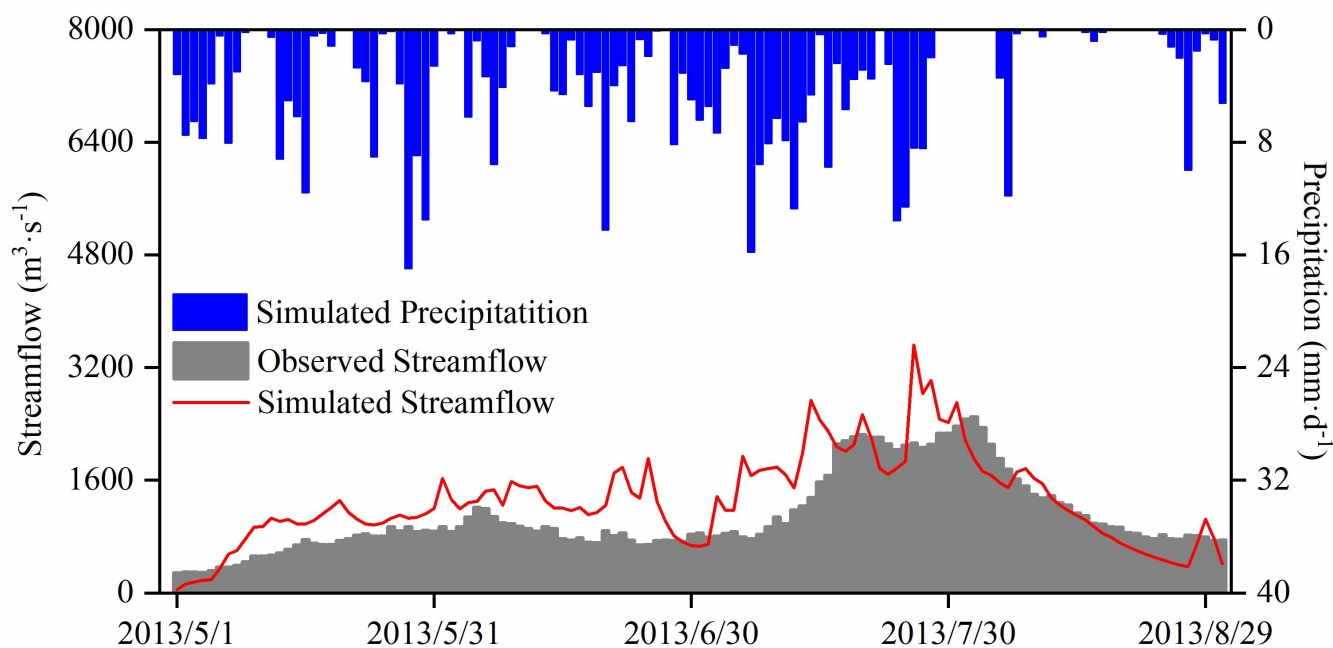
Figure 14. The observed and fully coupled WRF-Hydro simulated streamflow (units: $m^3 \cdot s^{-1}$) for the period May 1st, 2013 to
August 31st, 2013.

5 Discussion

388 The SRYR is rich in wetland resources and is the most important water conservation area in the middle and upper reaches of
389 the Yellow River, and the contribution of groundwater to surface runoff cannot be ignored (Jia et al., 2022). In this research,
390 the streamflow simulated by the uncoupled WRF-Hydro model is generally in good agreement with the observation.
391 However, the detailed portrayal of the hydrograph needs to be improved, especially the steep change of streamflow at the
392 flood peak, which does not well reflect the modulating effect of lateral flow of groundwater on streamflow changes.
393 Therefore, in order to clarify the mechanisms of groundwater and soil water content on streamflow, a comprehensive
394 analysis of land surface water cycle processes is supposed to be conducted in further research.

395 In addition, there is a significant overestimation of streamflow simulated by the fully coupled model in this research. To
396 better investigate the possible reasons for the degradation of the coupled simulation performance, the sensitivity analysis

plots of different atmospheric driving data combinations on the simulated streamflow from the uncoupled WRF-Hydro model are given in Fig. 15. The quality of precipitation data is very sensitive to streamflow simulations (WRFOUT) relative to the initial combination of driving data (GLDAS+CMFD) in this research, while non-precipitation data do not have a significant impact on streamflow (WRFOUT+CMFD). When using fully coupled simulated precipitation data, the slight deviations in precipitation (RMSE of 2.51 mm) cumulatively lead to larger error (458.85 $m^3·s^{-1}$) in the streamflow simulation. Therefore, reproducing daily streamflow with the fully coupled model remains a challenge at present (Li et al., 2021). Studies have shown that data assimilation has ability to improve the effect of precipitation forecasting at small and medium scales, promote the development of coupled atmosphere-land-hydrology simulation level, and is expected to further improve the accuracy of flood forecasting on the basis of extending the forecasting period (Gu et al., 2021). Therefore, satellite and radar data are able to be assimilated into the WRF model in the future research to improve the simulation results of the precipitation and streamflow. Meanwhile, the work of Senatore et al. (2015) is contribute to addressing the issue of the effect of different frequencies that the LSMs being called on streamflow simulation by enabling multiple time steps for different forcing and model components in the WRF-Hydro model.
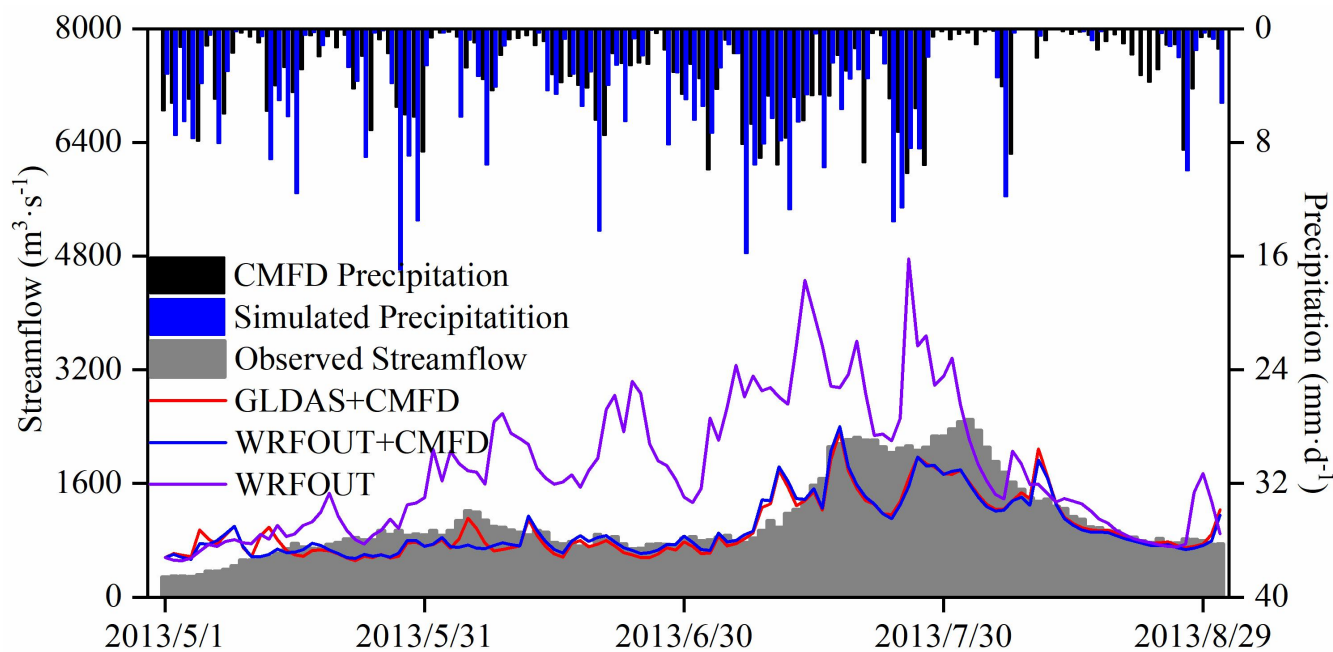
Figure 15. The uncoupled WRF-Hydro simulated streamflow (units: $m^3·s^{-1}$) driven by different precipitation data for the period May 1st, 2013 to August 31st, 2013.

23

6 Conclusions

Based on WRF-Hydro model, the meteorological, hydrological, eddy covariance stations and multiple reanalysis data over the SRYR, the key variables of the coupled atmosphere-land-hydrological processes simulated by standalone WRF and coupled WRF-Hydro model during the 2013 rainy season (May-August) are compared and analyzed to investigate the effects of climate change on land surface and water cycle processes and the feedback of land surface hydrological cycle to precipitation over the SRYR in this research. The following conclusions have been drawn:

1) The uncoupled WRF-Hydro model is able to characterize the variability of streamflow over the SRYR basin with a R of 0.84 and a NSE of 0.44 for the simulated streamflow and observations during the calibration period, and a R of 0.81 and a NSE of 0.61 for the validation period.

2) In terms of temporal variation, both the results of the standalone WRF and the coupled WRF-Hydro model indicate the reasonable performance in reproducing variables of atmospheric-land-hydrological processes over the SRYR. Compared with WRF model, the coupled process improves the simulation results for temperature, downward longwave and shortwave radiation, but slightly increases the wet bias of the precipitation and evapotranspiration, with a RMSE increased from 2.50 to 2.51 mm for precipitation and from 0.71 to 0.78 mm for evapotranspiration. Due to the consideration of lateral flow of soil water, the coupling process significantly reduces the bias of the simulation results of water-heat exchange fluxes, soil temperature and moisture, with a mean RMSE of 32.27 $W \cdot m^{-2}$, 24.91 $W \cdot m^{-2}$, 4.22 K, and 0.06 m^3/m^3 respectively.

3) In terms of spatial distribution, the coupled simulation increases the wet bias of the precipitation with a mean wet bias of 16.63 mm than WRF simulations, which is caused by the lateral redistribution and reinfiltration of soil water, but slightly enhance the simulation results of temperature. The coupled process increases the LE and overcomes the problem of large H simulation, and also results in a slight wetting and cooling of the near-surface atmosphere, making the spatial distribution of water-heat exchange flux and soil temperature and moisture more reasonable.

4) The fully coupled model is able to capture the variation characteristics of streamflow. However, reproducing daily streamflow with the fully coupled model remains a challenge, with a NSE of 0.33 and RMSE of 458.85 $m^3 \cdot s^{-1}$, because of the uncertainty of the simulated precipitation.

444 soil temperature and moisture data of the Eling Lake station from the National Cryosphere Desert Data Center

445 (http://www.ncdc.ac.cn, Meng and Lyu, 2022). The CMFD data are provided by the National Tibetan Plateau Data Center

446 (https://doi.org/10.11888/AtmosphericPhysics.tpe.249369.fle, He et al., 2020). The GLDAS data are from

447 https://ldas.gsfc.nasa.gov/gldas/ (Beaudoing and Rodell, 2020).

448 **Author contributions**. YC and WJ mainly wrote the manuscript and were responsible for the research design, data

449 preparation and analysis. XM provided critical insights to the research results. And the other authors discussed and assisted

450 with interpretation of the results and contributed to the article. All authors have read and agreed to the published version of

451 the manuscript.

452 **Competing interests**. The authors declare that they have no conflict of interest.

459 **References**

460 An, Y. Y.; Meng, X. H.; Zhao, L.; Li, Z. G.; Lyu, S. H.; Ma, Y. T.: Evaluation the applicability of albedo products of

461 　　　GLASS, MODIS and GlobAlbedo under the alpine meadow over the Qinghai-Tibetan Plateau, Plateau Meteor.,

462 　　　38, 88-100, https://doi.org/10.7522/j.issn.1000-0534.2018.00097, 2019.

463 An, Y. Y.; Meng, X. H.; Zhao, L.; Li, Z. G., Wang, S. Y., Shang, L. Y., Chen, H., Lyu, S. H., Li, G. W., and Ma, Y. S.:

464 　　　Performance of GLASS and MODIS Satellite Albedo products in diagnosing Albedo variations during different

465 　　　time scales and special weather conditions in the Tibetan Plateau, Remote Sens., 12, 2456,

466 　　　https://doi.org/10.3390/rs12152456, 2020.

467 Arnault, J., Wagner, S., Rummler, T., Fersch, B., Bliefernicht, J., Andresen, S., and Kunstmann, H.: Role of runoff-

468 　　　infiltration partitioning and resolved overland flow on land-atmosphere feedbacks: A case study with the WRF-

469 　　　Hydro coupled modeling system for west Africa, J. Hydrometeorol., 17, 1489-1516, https://doi.org/10.1175/JHM-

470 　　　D-15-0089.1, 2016.

471 Beaudoing, H. and M. Rodell, NASA/GSFC/HSL: GLDAS Noah Land Surface Model L4 3 hourly 0.25 x 0.25degree

472 　　　V2.1, Greenbelt, Maryland, USA, Goddard Earth Sciences Data and Information Services Center (GES DISC),

473   Accessed: [2022-11-23], 10.5067/E7TYRXPJKWOQ, 2020.

474   Chen, Y. L., Wen, J., Yang, C. G., Long, T. P., Li, G. W., Jia, H. J., and Liu, Z.: Analysis on the applicability of

475   different precipitation products and WRF-Hydro model over the Source Region of the Yellow River, Chinese

476   Journal of Atmospheric Sciences, [preprint], https://doi.org/10.3878/j.issn.1006-9895.2205.22057, 2020.

477   Clark, M. P., Fan, Y., Lawrence, D. M., Adam, J. C., Bolster, D., Gochis, D. J., et al.: Improving the representation of

478   hydrologic processes in Earth System Models, Water Resour. Res., 51, 5929–5956,

479   https://doi.org/10.1002/2015WR017096, 2015.

480   Cuo, L.; Zhang, Y. X.; Gao, Y. H.; Hao, Z. C.; and Cairang, L.S.: The impacts of climate change and land cover/use

481   transition on the hydrology in the upper Yellow River Basin, China. J. Hydrol. 502, 37-52,

482   https://doi.org/10.1016/j.jhydrol.2013.08.003, 2013.

483   Fersch, B., Senatore, A., Adler, B., Arnault, J., Mauder, M., Schneider, K., Voelksch, I., and Kunstmann, H.: High-

484   resolution fully coupled atmospheric-hydrological modeling: A cross-compartment regional water and energy

485   cycle evaluation, Hydrol. Earth Syst. Sci., 24, 2457-2481, https://doi.org/10.5194/hess-24-2457-2020, 2020.

486   Gharamti, M. E., McCreight, J. L., Noh, S. J., Hoar, T. J., RafieeiNasab, A., and Johnson, B. K.: Ensemble streamflow

487   data assimilation using WRF-Hydro and DART: novel localization and inflation techniques applied to Hurricane

488   Florence flooding, Hydrol. Earth Syst. Sci., 25, 5315-5336, https://doi.org/10.5194/hess-25-5315-2021, 2021.

489   Gochis, D. J., and Chen, F.: Hydrological enhancements to the community Noah land surface model (No. NCAR/TN-

490   454+STR). University Corporation for Atmospheric Research, https://doi.org/10.5065/D60P0X00, 2020.

491   Grell G. A., and Devenyi, D.: A generalized approach to parameterizing convection combining ensemble and data

492   assimilation techniques, 29, 38-1-38-4, https://doi.org/10.1029/2002GL015311, 2002.

493   Gu, T. W., Chen, Y. D., Gao, Y. F., Qin, L. Y., Wu, Y. Q., and Wu, Y. Z.: Improved streamflow forecast in a small-

494   medium sized river basin with coupled WRF and WRF-Hydro: Effects of radar data assimilation, Remote Sensing,

495   13, 3251, https://doi.org/10.3390/rs13163251, 2021.

496   He, J., Yang, K., Tang, W. J., Lyu, H., Qin, J., Chen, Y. Y., and Li, X.: The first high-resolution meteorological

497   forcing dataset for land process studies over China, Sci Data, 7, 25, https://doi.org/10.1038/s41597-020-0369-y,

498   2020.

499   Iacono, M. J., Delamere, J, S., Mlawer, E. J., Shephard, M. W., Clough, S. A. and Collins, W. D.: Radiative forcing by

500   long-lived greenhouse gases: Calculations with the AER radiative transfer models, 113, D13,

501   https://doi.org/10.1029/2008JD009944, 2008.

502   Ji, P., Yuan, X., Ma, F., and Pan, M.: Accelerated hydrological cycle over the Sanjiangyuan region induces more

503   streamflow extremes at different global warming levels, Hydrol. Earth Syst. Sci., 24, 5439-5451,

504   https://doi.org/10.5194/hess-24-5439-2020, 2020.

505 Jia, D. Y., Wen, J., Zhang, T. T., and Xi, J. J.: Response of soil water content and soil thermal conductivity on
506   precipitation in Loess Plateau, 33, 712-720, https://doi.org/10.7522/j.issn.1000-0534.2014.00049, 2014.

507 Jia, S. F., Liang, Y., and Zhang, S.F.: Discussion on evaluation of natural runoff in the Yellow River Basin, Water
508   Resources Protection, 38, 33-38+55, https://doi.org/10.3880/j.issn.1004 6933.2022.04.006, 2022.

509 Kruk, N. S., Vendrame, I. F., and Chou, S. C.: Coupling a mesoscale atmospheric model with a distributed
510   hydrological model applied to a watershed in Southeast Brazil, Journal of Hydrologic Engineering, 18, 58-65,
511   https://doi.org/10.1061/(ASCE)HE.1943-5584.0000606, 2012.

512 Li, G. W., Meng, X. H., Blyth, E., Chen, H., Shu, L. L., Li, Z. G, Zhao, L., and Ma, Y. M.: Impact of fully coupled
513   hydrology-atmosphere processes on atmosphere conditions: Investigating the performance of the WRF-Hydro
514   model in the Three River Source Region on the Tibetan Plateau, China, Water, 13, 3409,
515   https://doi.org/10.3390/w13233409, 2021.

516 Li, X., Gao, Y. H., Wang, W. Z., Lan, Y. C., Xu, J. W., and Li, K.: Climate changes and applicability of GLDAS in the
517   headwater of the Yellow River Basin. Advances in Earth Science, 29, 531-540,
518   https://doi.org/10.11867/j.issn.1001-8166.2014.04.0531, 2014.

519 Meng, X. H., and Lyu, S. H.:Turbulent flux observation data at the lakeside observation site in the Euling Lake basin
520   (2013), National Cryosphere Desert Data Center (www.ncdc.ac.cn),
521   https://doi.org/10.12072/ncdc.ZPWERS.db2031.2022, 2022.

522 Meng, X. H., Chen, H., Li, Z. G., Zhao, L., Zhou, B. R., Lyu, S. H., Deng, M S., Liu, Y M., and Li, G. W.: Review of
523   Climate Change and Its Environmental Influence on the Three-River Regions, Plateau Meteorology, 39, 1133-
524   1143, https://doi.org/10.7522/j.issn.1000-0534. 2019.00144, 2020.

525 Milly, P. C. D., Wetherald, R. T., Dunne, K. A., and Delworth, T. L.: Increasing risk of great floods in a changing
526   climate, Nature, 415, 514–517, https://doi.org/10.1038/415514a, 2002.

527 Milly, P. C. D., Dunne, K. A., and Vecchia, A. V.: Global pattern of trends in streamflow and water availability in a
528   changing climate, Nature, 438, 347–350, https://doi.org/10.1038/nature04312, 2005.

529 Nakanishi, M., and Niino, H.: An Improved Mellor–Yamada Level-3 Model: Its Numerical Stability and Application
530   to a Regional Prediction of Advection Fog, Boundary-Layer Meteorol, 119, 397-407,
531   https://doi.org/10.1007/s10546-005-9030-8, 2006.

532 Niu, G. Y., and Coauthors.: The community Noah land surface model with multiparameterization options (Noah-MP):
533   1. Model description and evaluation with local-scale measurements, J. Geophys. Res.: Atmos., 116, D12109,
534   https://doi.org/10.1029/2010JD015139, 2011.

535 Niu, G. Y., and Yang, Z. L.: Effects of frozen soil on snowmelt runoff and soil water storage at a continental scale, J.
536   Hydrometeorol., 7, 937-952, https://doi.org/10.1175/JHM538.1, 2006.

537 Senatore, A., Mendicino, G., Dochis, D. J., Yu, W., Yates, D. N., and Kunstmann, H.: Fully coupled atmosphere-
538   hydrology simulations for the central Mediterranean: Impact of enhanced hydrological parameterization for short
539   and long time scales, J. Adv. Model. Earth. Sy., 7, 1693-1715, https://doi.org/10.1002/2015MS000510, 2015.

540 Sheng, M.Y.; Lei, H.M.; Jiao, Y.; and Yang, D.W.: Evaluation of the runoff and river routing schemes in the
541   community land model of the Yellow River Basin, J. Adv. Modeling Earth Syst., 2993-3018,
542   https://doi.org/10.1002/2017MS001026, 2017.

543 Song, Y. M., Wang, Z. F., Huang, A. N.: Soil moisture memory and its effect on the surface water and heat fluxes on
544   seasonal and interannual time scales, J. Geophys. Res.: Atmos., 124, 10730-10741,
545   https://doi.org/10.1029/2019JD030893, 2019.

546 Skamarock, W. C.; Klemp, J. B.: A time-split nonhydrostatic atmospheric model for weather research and forecasting
547   applications, J. Comput. Phys., 227, 3465-3485, https://doi.org/10.1016/j.jcp.2007.01.037, 2008.

548 Tang, Q. H., Liu, X. C., Li, Z.,Yun, X. B., Zhang, X. J., Yu, Q., Li, J., Zhang, Y. Y., Cui, H. J., Sun, S. A., Zhang, C.,
549   Tang, Y., and Leng, G. Y.: Integrated water systems model for terrestrial water cycle simulation, Advances in
550   Earth Science, 34, 115-123. https://doi.org/10.11867/j.issn.1001-8166.2019.02.0115, 2019.

551 Thompson, G., Field, P. R., Rasmussen, R. M., and Hall, W. D.: Explicit Forecasts of Winter Precipitation Using an
552   Improved Bulk Microphysics Scheme. Part II: Implementation of a New Snow Parameterization, 136, 5095-5115,
553   https://doi.org/10.1175/2008MWR2387.1, 2008.

554 Wang, J., Liu, D. W., Tian, S. N., Hu, Y. H., Ma, J. L., and Wang, L. X.: Coupling analysis of short-term weather and
555   runoff in an arid lake basin of China. Regional Sustainability, 2, 264-279,
556   http://regsus.xjegi.com/EN/10.1016/j.regsus.2021.11.005, 2021.

557 Wen, J., Lan, Y. C., Su, Z. B., Tian, H., Shi, X. K., Zhang, Y., Wang, X., Liu, R., Zhang, T. Y., Kang, Y., Lyu, S. N.,
558   and Zhang, J. H.: Advances in observation and modeling of land surface process over the Source Region of the
559   Yellow River, Advances in Earth Science, 26, 575-585, https://doi.org/10.11867/j.issn.1001-8166.2011.06.0575,
560   2011.

561 Wu, G. X., Mao, J. Y., Duan, A. M., and Zhang, Q.: Recent progressing in the study on the impacts of Tibetan Plateau
562   on Asian summer climate, Acta Meteorologica Sinica, 62, 528-549, https://doi.org/CNKI:SUN:QXXB.0.2004-05-
563   002, 2004.

564 Yang, Y. Z., Yuan, H. L. and Yu, W.: Uncertainties of 3D Soil Hydraulic Parameters in Streamflow Simulations using
565   a Distributed Hydrological Model System, J. Hydrol., 567, 12-24, https://doi.org/10.1016/j.jhydrol.2018.09.042,
566   2011.

567 Taylor, K. E.: Summarizing multiple aspects of model performance in a single diagram. J. Geophys. Res., 106, 7183-
568   7192, https://doi.org/10.1029/2000JD900719, 2011.

569   Ye, D., Zhang, S. W, Wang, F. Y., Mao, F. P., and Yang, X. X.: The applicability of different parameterization

570   schemes in semi-arid region based on Noah-MP land surface model, Chinese Journal of Atmospheric Sciences, 41,

571   189-201, https://doi.org/10.3878/j.issn.1006-9895.1604.15226, 2017.

572   Yuan, X., Ji, P., Wang, L. Y., Liang, X. Z., Yang, K., Ye, A. Z., Su, Z. B., & Wen, J.: High-resolution land surface

573   modeling of hydrological changes over the Sanjiangyuan region in the eastern Tibetan plateau: 1. Model

574   development and evaluation, Journal of Advances in Modeling Earth Systems, 10, 2806-2828,

575   https://doi.org/10.1029/2018MS001413, 2018.

576   Yucel, I., Onen, A., Yilmaz, K. K., and Gochis, D. J.: Calibration and evaluation of a flood forecasting system: Utility

577   of numerical weather prediction model, data assimilation and satellite-based rainfall, J. Hydrol., 523, 49-66,

578   https://doi.org/10.1016/j.jhydrol.2015.01.042, 2015.

579   Zhang, A., Li, T. J., Fu, W., and Wang, Y. T.: Model simulation of flood season runoff in the headwaters of the

580   Yellow River Basin using satellite-ground merged precipitation data, Journal of Basic Science and Engineering,

581   25, 1-16, https://doi.org/10.16058/j.issn.1005-0930.2017.01.001, 2017.

582   Zhang, H. X., N. M. Yuan, Z. G. Ma, and Y. Huang.: Understanding the soil temperature variability at different depths:

583   Effects of surface air temperature, snow cover, and the soil memory. Adv. Atmos. Sci., 38, 493-503,

584   https://doi.org/10.1007/s00376-020-0074-y, 2021.

585   Zhang, Q., Wen, J., Zhang, T. T., Yang, Y. T., Wu, Y. Y., Zhang, G., Liu, W. H., Chen, Y. L., and Yan, Z. T.: The

586   impacts of roughness length on the simulation of land-atmosphere water and heat exchanges over the Yarlung

587   Zangbo Grand Canyon region, Front. Earth Sci., https://review.frontiersin.org/review/1077791/18/2102738#/.

588   Zhang, Z.; Arnault, J.; Wagner, S.; Laux, P.; and Kunstmann, H.: Impact of lateral terrestrial water flow on land-

589   atmosphere interactions in the Heihe River Basin in China: Fully Coupled Modeling and Precipitation Recycling

590   Analysis, J. Geophys. Res. Atmos., 124, 8401-8423, https://doi.org/10.1029/2018JD030174, 2019.

591   Zheng, D.; van der Velde, R.; Su, Z.; Wen, J.; Wang, X.; and Yang, K.: Impact of soil freeze-thaw mechanism on the

592   runoff dynamics of two Tibetan rivers, J. Hydrol., 563, 382-394, https://doi.org/10.1016/j.jhydrol.2018.06.024,

593   2007.

594   Zheng, H. X., Zhang, L., Liu, C. M., Shao, Q. X., and Fukushima, Y.: Changes in stream flow regime in headwater

595   catchments of the Yellow River basin since the 1950s, Hydrol. Process, 21, 886-893,

596   https://doi.org/10.1002/hyp.6280, 2006.

597   Zheng, Z. Y., Lyu, M. X., and Ma, Z. G.: Climate, Hydrology, and Vegetation Coverage Changes in Source Region of

598   Yellow River and Countermeasures for Challenges, Bulletin of Chinese Academy of Sciences, 35, 61-72,

599   https://doi.org/10.16418/j.issn.1000-3045.20191230002, 2020.